Global and Planetary Change 223 (2023) 104090

Contents lists available at ScienceDirect

Global and Planetary Change

journal homepage: www.elsevier.com/locate/gloplacha

Research Article

Coupled kinematic and thermal modelling of collisional orogens: Implications for subsurface geo-resources assessment in the external Dinarides

F.H. Nader [a,b,*], M. van Unen [b,c], R. Darnault [a], J.-L. Rudkiewicz [a], L. Matenco [b]

[a] IFP Energies Nouvelles, Earth Sciences and Environmental Technologies Division, Rueil-Malmaison, France
[b] Utrecht University, Department of Earth Sciences, Utrecht, The Netherlands
[c] TNO, Energy & Materials Transition Unit, the Netherlands

ARTICLE INFO

Editor: Dr. Howard Falcon-Lang

Keywords:
Kinematic
Heat flow
Thin-skinned
Seismic interpretation
Coupled modelling
Geothermal
TOC
Petroleum systems

ABSTRACT

The thermal evolution of collisional orogens is largely controlled by their kinematic and burial/exhumation history, where sedimentation and erosion rates, as well as shear heating and deep heat flow supply conditions for the temperature distribution, fluid flow and the associated fluid-rock interactions. The aim of our research is to understand this coupled kinematic and thermal evolution to ultimately infer the conditions favourable for subsurface geo-resources. We achieve this aim by means of numerical modelling and its application to one of the best available orogenic indentation examples, which is the Dinarides Mountains chain in Central Europe. Based on the analysis and modelling of an integrated onshore and offshore geological cross-section, we quantified the shortening, erosion/exhumation and sedimentation/burial rates, maturity of potential petroleum source rocks and the gross potential for sustainable geothermal resources. The coupled kinematic/thermal modelling revealed a general pattern of heat flow variations associated with crustal deformations. The hanging-wall and upper parts of the footwalls show increased conductivity and heat flow during episodes of thrusting, whereas the deepest parts of footwalls have lower heat flow values. Fluids are observed to migrate towards the foreland during the latest Cretaceous – Early Oligocene thrusting. The largest amounts of post-Middle Miocene shortening took place in the SE external parts of the orogen, where deep-sourced fluid ascent took place towards the foreland. In this region, significant footwall burial enhanced the maturation of potential source rocks. Modelling results infer a considerable hydrocarbon potential for the Dalmatian unit and the South Adriatic basin. The kinematic and thermal model combined with geothermal well design and well performance calculations infer a viable geothermal energy potential for the Dalmatian and High-Karst units. Results of this novel workflow allowed to quantify the orogenic kinematic and thermal history, and its bearing on conventional and sustainable geo-resources.

1. Introduction

Collisional orogens commonly involve crustal accretion mechanisms during the migration of subduction zones and contractional deformation towards the orogenic foreland or hinterland, influenced by the evolution of subducted slabs (Doglioni et al., 2007; Duretz and Gerya, 2013; England and Houseman, 1986; Rosenberg et al., 2018; Tapponnier et al., 1986). The foreland-ward migration of contractional deformation and accretion can be associated with *syn-* and post-tectonic exhumation, erosion and/or extension in the inner part of the tectonic wedge (Ballato et al., 2019; Beaumont, 1981; Beaumont et al., 1990; Platt, 1986; Vogt et al., 2017). The associated erosion and sedimentation rates, as well as shear heating and deep heat flow supply are the main processes controlling the temperature distribution, fluid flow and the location of subsurface geo-resources in such collisional orogens (Huerta and Rodgers, 2006; Leloup et al., 1999; Nemčok et al., 2005; Roure et al., 1993; Spooner et al., 2020; Willett and Brandon, 2002).

The coupling of kinematic evolution with fluid flow, diagenesis and the potential for geo-resources has been extensively studied but remains a domain where the quantitative assessment is still less developed (e.g., Ferket et al., 2011; Roure et al., 2005; Vilasi et al., 2009). The difficulty relates to the lack of subsurface data and calibration constraints, as well

* Corresponding author at: IFP Energies Nouvelles, Rueil-Malmaison, France.
E-mail address: fadi-henri.nader@ifpen.fr (F.H. Nader).

https://doi.org/10.1016/j.gloplacha.2023.104090
Received 29 November 2022; Received in revised form 3 March 2023; Accepted 4 March 2023
Available online 11 March 2023

as adequate numerical tools for coupling such processes (e.g., Vilasi et al., 2009). Since the thermal evolution is conditioned also by the kinematic and burial/exhumation history in collisional settings (Davy and Gillet, 1986; Demetrescu and Andreescu, 1994; Dezes et al., 2004), they need to be tackled in a coupled manner in quantitative modelling procedures. The current approach is to first construct kinematic models that are subsequently used for a separated thermal analysis or modelling procedure (e.g., Spooner et al., 2020; Vilasi et al., 2009). Restoration methods, such as balanced cross-sections, have been applied to understand and quantify the evolution of structural geometries and kinematic relationships in collisional orogens (e.g., Balling et al., 2021b; Bally, 1981; Ellouz et al., 1994; Mitra and Boyer, 1986; Verges et al., 1995). These studies were applied on regional cross-sections and lead to better estimating the amounts of shortening, subsidence, and exhumation, as well as the temporal evolution of erosion and sedimentation. Such knowledge is also critical for thermal (basin) modelling in collisional settings, which estimates the evolution of porosity, heat transfer, as well as the generation and migration of conventional geo-resources such as hydrocarbons, accounting for the prevailing mechanisms of deformation (Cornu et al., 2003; Schneider, 2003). Basin modelling in orogenic areas is also relevant to the exploration of sustainable geo-resources (e.g., geothermal energy) and subsurface storage (e.g., CO_2, hydrogen, energy) activities (Boersma et al., 2021; Do Couto et al., 2021; Limberger et al., 2014).

The Dinarides Mountain chain in Central Europe, a collisional orogen where the deformation evolution through space and time has been recently quantified in detail, is a key place for the study of coupled kinematic and thermal evolution in orogens affected by indentation mechanics (Fig. 1, Matenco and Radivojević, 2012; Schmid et al., 2020; van Unen et al., 2019a). These previous studies have shown that following a Middle Triassic – Early Jurassic period of continental rifting, the contractional evolution has emplaced various oceanic and continental units starting from Late Jurassic times. The Late Cretaceous – Oligocene continental collision has emplaced a system of thick and thin-skinned nappes that are younger towards the foreland, but they do retain significant out-of-sequence deformation components (Fig. 2, Schmid et al., 2020; Stojadinovic et al., 2017; Ustaszewski et al., 2010). This collision was followed by a period of extension spanning throughout Late Oligocene - Middle Miocene times, which resulted in the formation of the Dinarides Lake System (e.g., Harzhauser and Mandic, 2008; Harzhauser et al., 2012; Mandic et al., 2012; Ustaszewski et al., 2010; van Unen et al., 2019b). Renewed contractional to transpressional deformation affected the Dinarides starting from the latest Miocene times (after ~9 Ma) in response to the large scale indentation of the Adriatic micro-continent, a deformation that remains active also at present (D'Agostino et al., 2020; Handy et al., 2019; Métois et al., 2015; van Unen et al., 2019a). Although the surface geometry and the regional kinematic history are well documented, the relationship between shortening and burial/exhumation during the tectonic evolution across the Dinarides remains largely unconstrained (Balling et al., 2021b), which has a large impact on the overall thermal evolution, reservoir properties and fluid-flow.

We aim to understand the coupled kinematic and thermal evolution of collisional orogens affected by indentation mechanics by the means of numerical modelling of the Dinarides evolution. This is achieved by building an integrated onshore and offshore orogenic transect that is subsequently modelled in a coupled kinematic and thermal approach. The research focusses on quantifying the differences in shortening rates, exhumation and burial rates, maturity of potential source rocks, as well as erosion and sedimentation rates. The impact of the coupled kinematic and thermal modelling constrained by the evolution of organic matter across the external Dinarides provides an integrated model of fluid-flow and heat transfer that can be extrapolated to similar collisional orogens worldwide. The practical application of the constructed modelling workflow not only helps in predicting hydrocarbons prospectivity in such complex orogens, but also provides input data that can be used to determine the technical performance of potential geothermal exploitation.

2. Tectono-stratigraphy, hydrocarbon systems and geothermal energy potential of the Dinarides

The NW-SE trending and SW-vergent Dinarides mountain chain connects the high convergence deformation recorded by the Alps with the Adriatic indentation and the rapid retreat of the Aegean slab and back-arc extension recorded by the Hellenides orogen (Fig. 1, e.g., Faccenna and Becker, 2020; Jolivet et al., 2021). The Upper Permian - lowermost Triassic strata in the Dinarides generally consist of shallow-marine carbonate sediments, continental sabkha clastics and evaporites. The evaporite deposits have been reported in the north-western Dinarides and were suggested to function locally as a decollement horizon for the subsequent thrusting (Fig. 3, Borojević Šoštarić and Kulušić, 2014; Grandić et al., 2010; Tari, 2002; Tišljar, 1992). Continental rifting occurred in the Middle Triassic, resulting in the opening of a northern branch of the Neotethys Ocean that separates Europe from Adria. This was associated with the creation of local (half-)grabens within the Adriatic domain, such as the Budva basin of Montenegro (Fig. 2, Cadjenovic et al., 2008; Goričan, 1994; Schmid et al., 2008; Stampfli and Borel, 2002; van Unen et al., 2019a).

The overall Triassic – Lower Eocene nappe in the external Dinarides is up to 9 km thick, consisting of shallow water sediments recorded over the Adriatic carbonate platform, with short periods of emergence in response to the interplay between eustatic changes and tectonics. The inferred shallow water depositional environment gradually deepens along the former passive continental margin, towards the more internal Dinaride units (Fig. 3, e.g., Dimitrijević, 1997; Korbar, 2009; Tišljar, 1992; Velić et al., 2015; Vlahovic et al., 2005). Locally, some areas show deeper facies and were interpreted to connect with the rifted structures of the Alps (e.g., the Belluno basin) or the Ionian basin (Bega, 2015; Goričan et al., 2012; Vlahovic et al., 2005). The Budva unit includes Lower Triassic - Middle Anisian shallow water carbonates (limestones and dolostones) that are intruded or overlain by rifting (sub-) volcanic bodies. The latter are laterally replaced and overlain by Upper Anisian - Lower Eocene deep-water nodular limestones, calcareous turbidites, radiolarites and other pelagic sediments that underly Middle – Upper Eocene clastic turbidites (Fig. 3, Cadjenovic et al., 2008; Crne et al., 2011; Dimitrijević, 1997; Goričan, 1994).

In the more internal Dinarides units, the Middle Jurassic Neotethys oceanic subduction was followed by the Late Jurassic – earliest Cretaceous obduction of the Western Vardar ophiolitic unit over the Adriatic passive margin and the deposition of Vranduk turbidites (Fig. 2). At almost the same time, shortening in the underlying continental unit prevailed until the end of Early Cretaceous times (Dimitrijević, 1997; Hrvatović, 2006; Mikes et al., 2008; Porkoláb et al., 2019; Robertson et al., 2009; Schmid et al., 2008). The latest Cretaceous – Oligocene continental collision was characterized by an overall migration of deformation to the more external areas of the Dinarides and deposition of *syn*-flexural sediments in the footwall of various nappe units, such as the uppermost Cretaceous Ugar-Durmitor turbidites in the footwall of the East Bosnian – Durmitor unit, or the Eocene - Oligocene turbidites (which pass to coarse shallow marine and continental deposits) in the footwall of many Dinarides thrusts (Figs. 2a and 3, e.g., Andrić et al., 2017; Dimitrijević, 1997; Hrvatović and Pamić, 2005; Stojadinovic et al., 2017; Ustaszewski et al., 2010). The end of contractional deformation is marked by the Upper Eocene – Oligocene shallow-water to alluvial continental regressive sequences dominated by coarse conglomerates, which are believed to demonstrate an out-of-sequence character of deformation (Fig. 3, Balling et al., 2021b; Mrinjek, 1993; Schmid et al., 2020; Zupanič and Babić, 2011). The overall style of deformation in the external Dinarides is a foreland and lateral transfer from thick- to thin-skinned SW-ward thrusting, whose exact character at depth is largely unknown, owing to the limited availability of subsurface

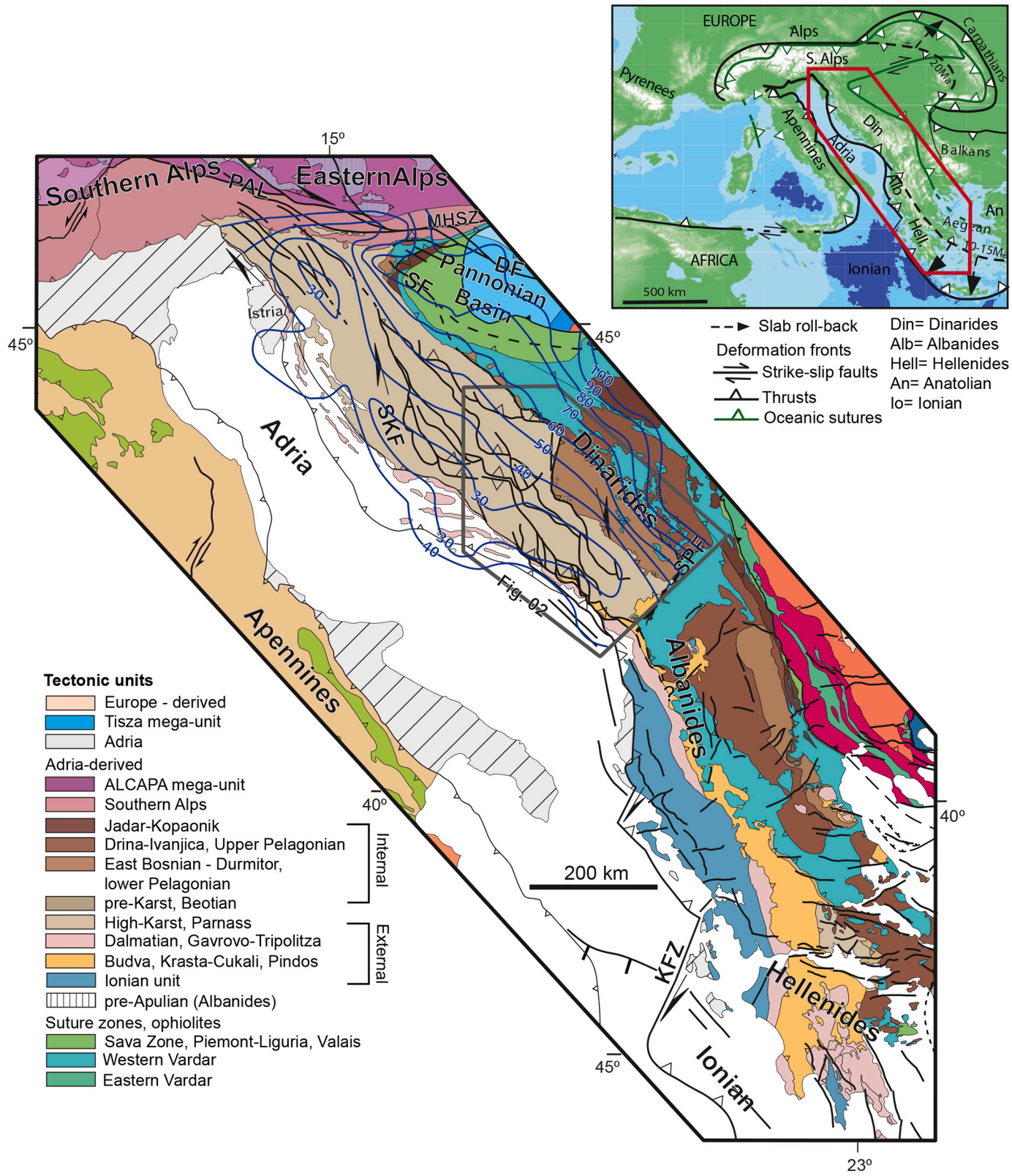

Fig. 1. Tectonic map of the external parts of the Dinarides, Albanides and Hellenides, as well as the neighbouring parts of Pannonian basin, Southern and Eastern Alps (after Schmid et al., 2008). In the Dinarides, the map is overlain by the post- 9 Ma fault system (Harzhauser and Mandic, 2008; Mandic et al., 2012; van Unen et al., 2019b). Blue lines represent the surface heat flow values in mW/m^2 (Milivojević and Martinović, 2005; Milivojević, 1993). The grey polygon is the location of the map in Fig. 2. The map in the upper right corner is the localization of the tectonic map in the larger European orogenic context. PAL = Peri – Adriatic Lineament; SKF = Split – Karlovac Fault; CHW = Cukali half-window; PW = Peshkopia Window. Dashed lines are locations of the orogenic front in the Carpathians and Aegean domain at 20 and 15 Ma, respectively (Wortel and Spakman, 2000). (For interpretation of the references to colour in this figure legend, the reader is referred to the web version of this article.)

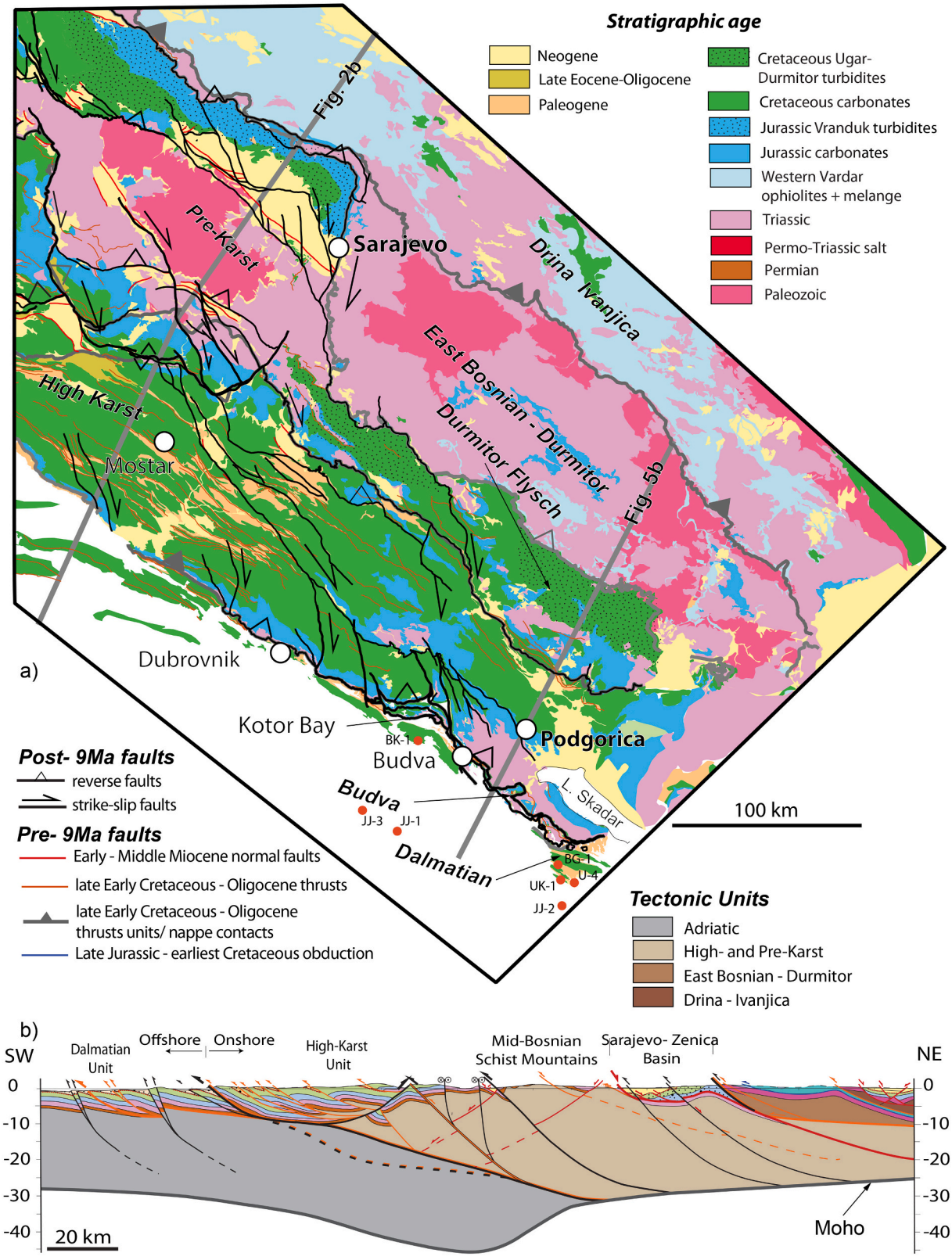

Fig. 2. a) Geological map of the central and south-eastern part of the Dinarides (simplified from 1:100.000 maps of former Yugoslavia – OGK, Osnova Geoloska Karta) overlaid by the post- 9 Ma fault system mapped in van Unen et al. (2019a, 2019b). Thick grey lines are major nappe contacts that have multiple ages across the orogen (pre-9 Ma). Red dots represent wells that were taken into account (together with seismic data) for the construction of the offshore cross-section in Montenegro. b) Regional structural cross-section at crustal-scale, trending NE-SW (see text for details and references). (For interpretation of the references to colour in this figure legend, the reader is referred to the web version of this article.)

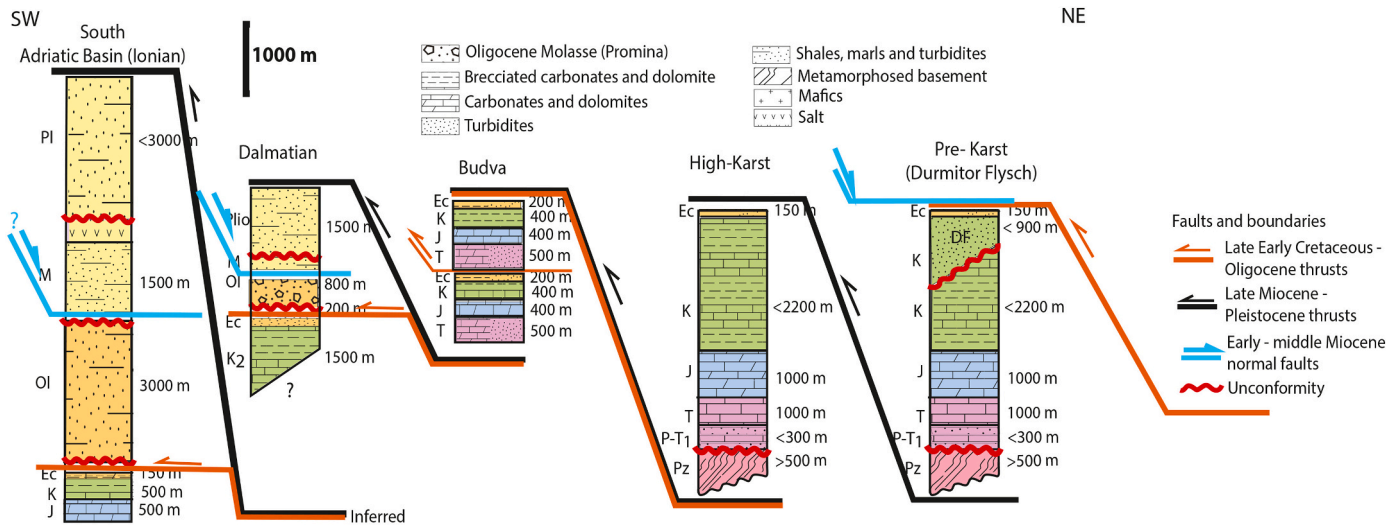

Fig. 3. Correlation of lithostratigraphic columns along the various tectonic units of the investigated geologic section, from Pre-karst to South Adriatic basin domains (NE to SW, respectively; from van Unen et al., 2019b). Thickness values are average.

information in the onshore (Fig. 2b, e.g., van Unen et al., 2019a). In the Dalmatian unit, the latest Cretaceous – Oligocene thrusting was associated with a local flexural unconformity between Cretaceous and Paleocene carbonate strata, a local erosion of Upper Paleocene to Oligocene clastics in the hanging-wall of thrusts, and a flexural basin in the Adriatic footwall, infilled with up to 4 km thick Paleogene clastics (Fig. 3, Bega, 2015; Velić et al., 2015).

The onset of extension, towards the end of Oligocene, partly coeval with the extension in the neighbouring and larger Pannonian basin, led to the formation of numerous basins with dominantly half-graben structures, mostly of Early-Middle Miocene age. These structures often include reactivated pre-existing thrusts or nappe contacts, such as the ones that are observed in the larger Sarajevo-Zenica basin (Fig. 2, Andrić et al., 2017; van Unen et al., 2019a; Žibret and Vrabec, 2016). The extension peak occurred around 15–14 Ma, resulting in the formation of the Dinarides Lake System, an endemic and isolated group of intramontane lakes that overlies the previous orogenic structure. The areal extent of the Dinarides Lake System was further enhanced by the Miocene Climatic Optimum with the associated marine flooding and sedimentation extending until around 9 Ma (Figs. 2 and 3, de Leeuw et al., 2012; Harzhauser and Mandic, 2008; Harzhauser et al., 2012; Mandic et al., 2012). The onset of the Adriatic indentation took place after 9 Ma and was accompanied by the exhumation of many of these extensional structures, through the creation of a complex fault system distributing transpressional (mostly dextral strike-slip) and contractional deformation obliquely across the Dinarides orogen (Fig. 2a, Balling et al., 2021a; van Unen et al., 2019a). This fault system connects the shortening and strike-slip deformations that are observed in the internal Dinarides (near the Alps) with similar deformations in the external Dinarides, near the Albanides and Hellenides; (Fig. 1, Handy et al., 2019; Moulin et al., 2016; Schmitz et al., 2020; Tomljenović et al., 2008; Vrabec and Fodor, 2005). Furthermore, this fault system closely mirrors the present-day seismicity, stress field and horizontal motions in the Dinarides and neighbouring areas that have been interpreted to be driven by the Adriatic indentation mechanics (D'Agostino et al., 2020; Métois et al., 2015; van Unen et al., 2019a; Weber et al., 2010). The Adriatic foreland basin in Montenegro and Albania offshore, includes up to 1.5 km thick Miocene clastics, with an unconformity and thin sedimentation interval ascribed to the Messinian Salinity Crisis (Fig. 3, Bega, 2015; Bertotti et al., 2001; Roure et al., 2004; Vilasi et al., 2009). These clastics are overlain by Pliocene-Quaternary clastics with thicknesses reaching up to 3 km.

The presence of thin- and/or thick-skinned structures in the offshore SE Dinarides affecting the South Adriatic basin is believed to have important sub-thrust trapping potential for hydrocarbon exploration (Bega, 2015; Bertotti et al., 2001; Dragasević, 1983; Picha, 2002; Zappaterra, 1994). Such sub-thrust structures have not yet been confirmed by drilling in offshore Montenegro, but their possible occurrence is promoted by the interpretation of a limited number of onshore and offshore reflection seismic profiles and gravity data. Furthermore, structural seismic interpretations and stratigraphic correlation with wells led to inferring several viable petroleum systems in offshore and neighbouring onshore areas (e.g., Bega, 2015). Regional, deep seismic profiles onshore calibrated by wells remain fundamental for imaging the subsurface thrusting geometries and for deriving the extent of the initial Late Triassic – Early Jurassic Budva extensional basin.

The known petroleum potential in the SE-Dinarides includes four principal source rocks, three reservoir and four seal intervals (Bega, 2015; Dubljević, 2008; Gušić and Jelaska, 1993; Velaj, 2012; Zappaterra, 1994). The source rocks include the Anisian pelagic sediments and turbidites (primary oil source) with TOC values of up to 0.7%, the Upper Cretaceous - Middle Eocene shales and marls (oil and gas-prone) with up to 1.5% TOC, the Eocene - Oligocene shales (mainly gas prone) with up to 3.9% TOC and the Lower Pliocene shales (biogenic gas sources) (Fig. 4). Potential reservoir intervals are the Cretaceous-Eocene shelf edge and platform carbonates, Oligocene-Lower Pliocene turbidites, and Miocene - Pleistocene siliciclastics (Fig. 4). Potential sealing units include overthrusted Permo-Triassic evaporites, Triassic shales, Oligocene and Miocene-Pleistocene intra-formational deep marine shales (Fig. 4). Permo - Triassic evaporites were also encountered in onshore wells (e.g., UK-1 and Mo-1, Bega, 2015).

The eastern, internal part of the Dinarides includes tens of viable hydrogeothermal systems that have been characterized principally by various types of reservoirs (Milivojević and Martinović, 2005). The best reservoir/aquifer is the Triassic limestones and dolostones (>500 m thick), where the maximum water temperature at well-heads reaches 80 °C with discharge rates around 216 m^3/h (Milivojević, 1993). Such temperature and flow conditions make excellent geothermal energy systems for heating applications that fill an important societal need in the Montenegro regions of the High-Karst and East Bosnian Durmitor units. Temperatures around 80 °C can be reached in these units at depths <1.5 to 2 km (Milivojević, 1993). Such temperatures contrast with the relatively colder southwestern part of the Dinarides, where subsurface temperatures do not exceed 40 °C at similar depths.

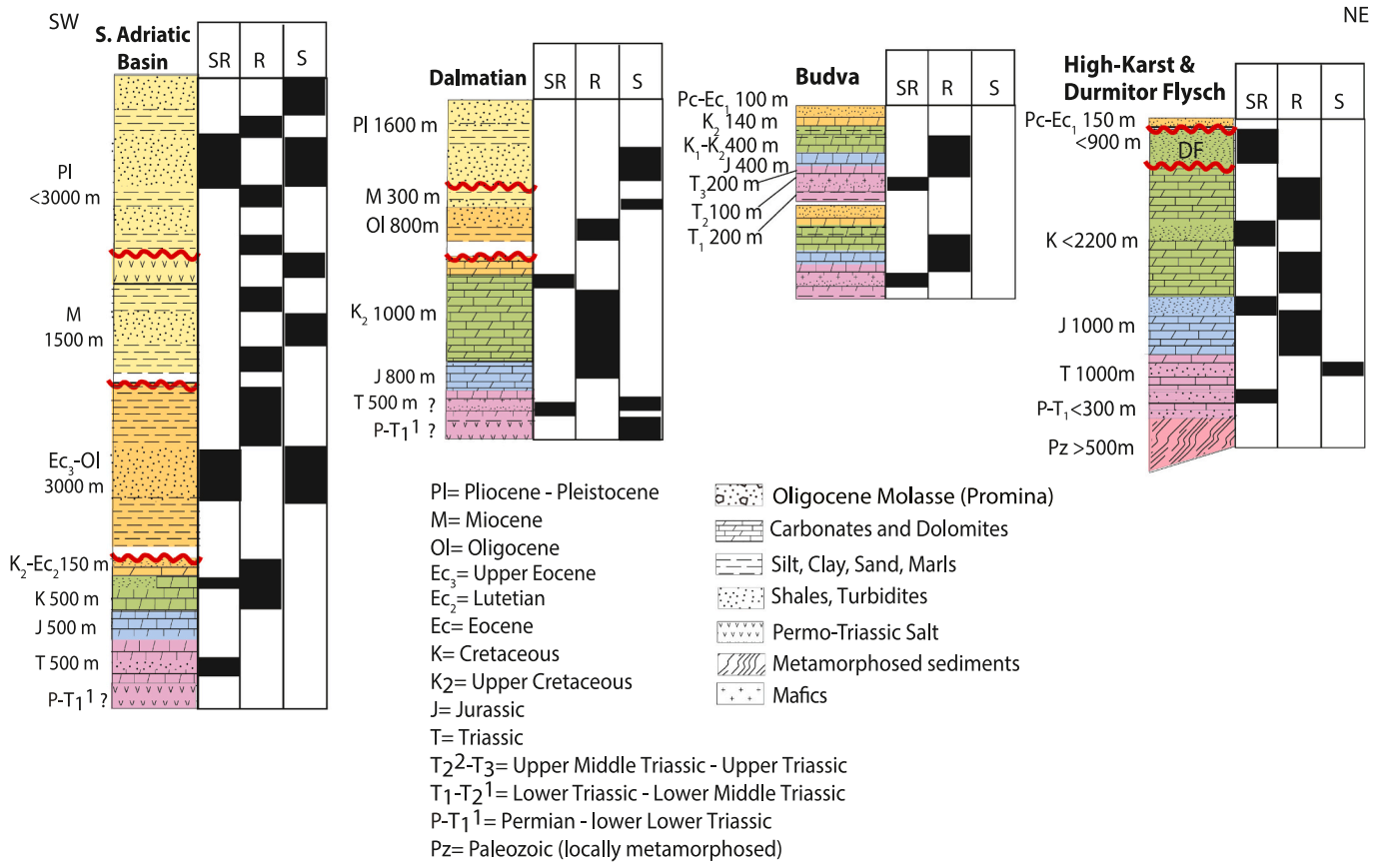

Fig. 4. Generalized lithostratigraphic columns along the main tectonic units, indicating source rock, reservoir rock and seal rock intervals (Grandić et al., 2010; Bega, 2015; Mazzuca et al., 2015; Velić et al., 2015).

3. Methodology

3.1. Seismic data (South Adriatic basin, offshore Montenegro)

Five 2D offshore two-way travel time seismic reflection profiles were available for this study, courtesy of the Montenegro Seismological Observatory and Montenegro Hydrocarbon Administration. We have selected one representative seismic line for constructing the regional correlation with the onshore (Fig. 2). The length of this seismic profile is 36 km and has a maximum depth of 9 s TWT (Fig. 5). The seismic interpretation consists of defining and tracing key horizons, while the thicknesses of the different interpreted stratigraphic units were derived from the neighbouring JJ-3 well (Fig. 2a; Bega, 2015). This well was also used to estimate seismic velocities and perform a time to depth conversion (Table 1).

3.2. Kinematic restorations and modelling

Kinematic restoration and modelling were performed on a 172 km long cross-section extending throughout the SE-Dinarides, from the East Bosnian-Durmitor unit in Serbia in the NE to the offshore Adriatic basin of Montenegro in the SW (Fig. 2). The minimum amounts of shortening and extension during the main episodes of deformation were quantified by restoring the large-scale structural features along this cross-section. Numerical restoration, accounting for the different deformation events and the associated kinematic and geometry evolutions, was performed by means of KronosFlow™ module of the OpenFlow Suite™ that provides a common numerical platform linking through a set of streamlined workflows advanced software modules (IFPEN and BeicipFranlab). The cross-section was subdivided into different fault-bound blocks with their own specific grid dimensions. The Moho geometry included in the constructed model is based on previously published interpretations derived from inverting Bouguer gravity data (Šumanovac, 2010), while the implementation of the Moho in the model accounts both rifting and shortening events.

Except for the Budva and Dalmatian units, the local presence of pre-Permian basement infers thick-skinned deformation. The faults depth prolongation and the connection with the Moho were drawn by structural and kinematic calculations, including along strike projections (see van Unen et al., 2019a, 2019b for details). Such projections have an increasing degree of uncertainty with depth. The algorithm used for restoring fault related deformation is the '*moving least square method*'. This method makes a global approximation of all available (unorganized) data points of the two sliding surfaces (both faults or horizons) and restores towards the region around the point for the best-fit reconstruction (Lancaster and Salkauskas, 1981). The '*flexural slip geometry driven method*' was also used to unfold extensional geometries. This method unfolds objects around a straight line, such as a fault, and preserves the area, volume, and line length (Dahlstrom, 1969). The mesh deformation, achieved by KronosFlow™, accounts for proper porous medium deformation, heat transfer, hydrocarbon generation and fluid migration, with no drawbacks on the scale nor the quality of the data obtained through further coupling with thermal (basin) modelling (TemisFlow™ module). De-compaction between two deformation phases for each step has been calculated, which allowed the related sediment geometries to adjust with unloading when going back in time.

3.3. Thermal/basin modelling

The 2D thermal/basin model of the restored cross-section was done with TemisFlow™ module of the OpenFlow Suite™ (IFPEN and BeicipFranlab). After simulating the evolving structural architecture

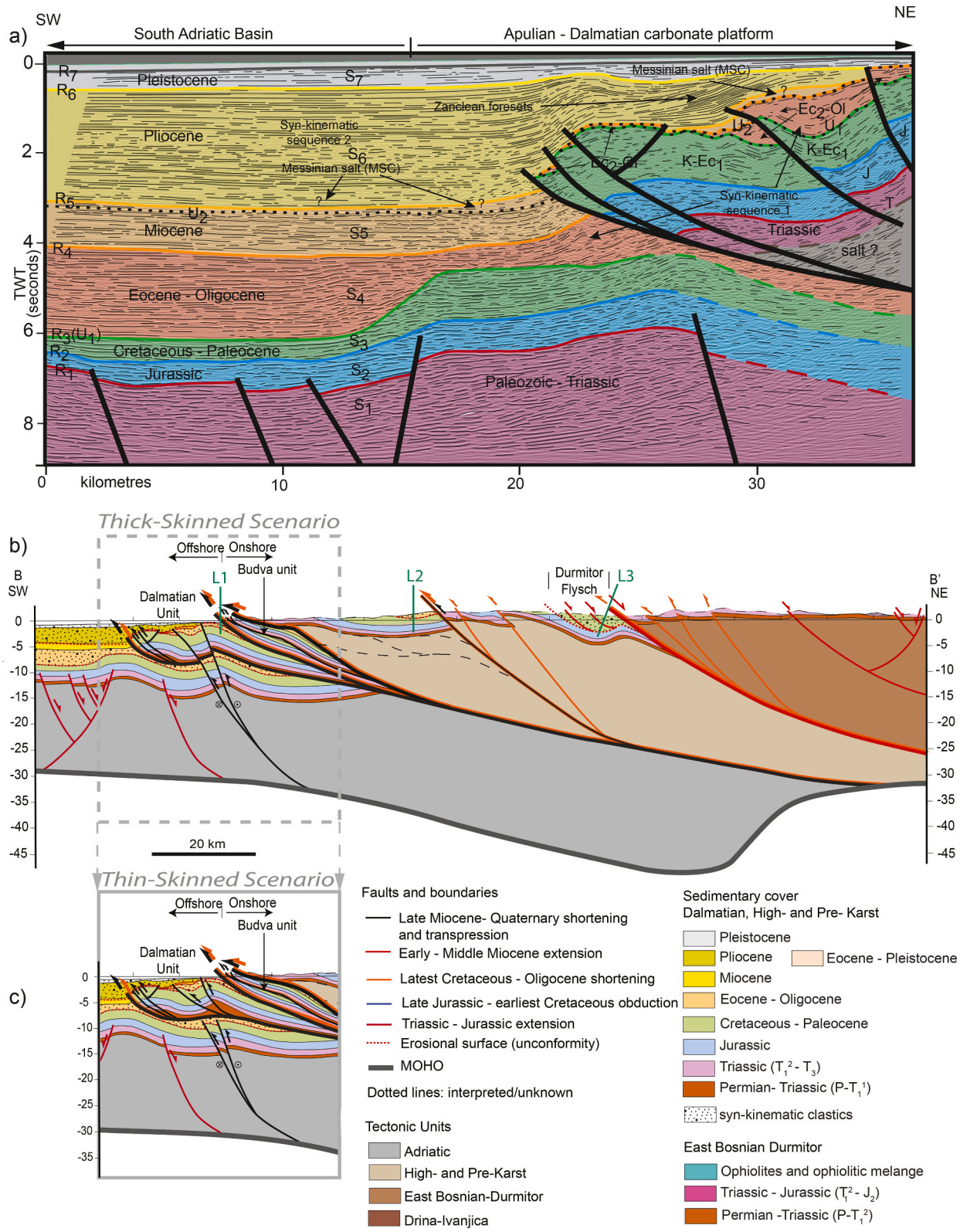

Fig. 5. a) Interpreted seismic line situated in offshore Montenegro (see text for details). The location of the seismic line is displayed in Fig. 2a. U = unconformities, R = horizons and S = stratigraphic packages. Ec2-Ol = middle Eocene-Oligocene, K-Ec1 = Cretaceous-lower Eocene. b) Regional orogenic cross-section (offshore-onshore) that extends from the South Adriatic basin in Montenegro to the East Bosnian-Durmitor in southern Serbia. The subsurface of the Dalmatian and Budva units is interpreted based on a thick-skinned deformation scenario. Three potential locations for geothermal doublets are indicated with a green line ([L1], [L2] and [L3]). c) An alternative scenario of thin-skinned deformation interpretation for the subsurface of offshore (Dalmatian) and onshore (Budva) margin. (For interpretation of the references to colour in this figure legend, the reader is referred to the web version of this article.)

Table 1
Velocity values for the most important seismic packages representing Mesozoic and Cenozoic sedimentary intervals. Estimated in m/s by dividing the sedimentary thicknesses in m from the JJ-3 well with the corresponding sedimentary thickness in seconds (TWT/2) from the seismic line Y-80-10E (from Bega, 2015).

Age / Sedimentary interval	Type of sediment	Velocity (m/s)
Pliocene – Pleistocene	Shales and sand	2062
Miocene	Shales and sand	2290
Oligocene	Shales and sand	2920
Paleocene	Carbonates	4000
Mesozoic	Carbonates	4374

through restoration, a simplified sedimentary/lithological filling was defined (based on existing lithostratigraphic information, Fig. 3) together with elements of potential petroleum systems (source rocks, reservoirs, seals). This approach is essential to model hydrocarbon generation and migration as well as fluid flow. The simplified lithological units of the 2D model are the Permo-Triassic shales and sand (50%/50%, except for the Dalmatian unit where the Permo-Triassic intervals consist of salt), Triassic dolostones, Jurassic and Cretaceous limestones, the Durmitor Flysch with shales and sands (50%/50%), and the Eocene to Pleistocene shales and sand (50%/50%). Porosity-depth laws are defined by a set of points for each lithological unit, representing porosity evolution controlled by both mechanical and chemical processes (TemisFlow™ database). Kozeny-Carman equation was used to define permeability spanning the full scale of porosity values for each lithological unit. Since the constructed model is 2D, the calculated evolution of relative permeability was used to infer the possible fluid flow through the sedimentary section. Within the basin model, faults transparent to fluid flow are assumed, which means that fluid flow along the faults only takes place when there is a juxtaposition between permeable layers. In contrast, when there is a juxtaposition between impermeable layers the fluids will not escape along the faults and are trapped within the permeable layers.

Thermal conditions strongly influence the physical and chemical properties of the source rocks and their associated maturity, as well as the properties of sediments and fluids. The heat flow distribution along the investigated cross-section depends on the tectonic processes, mantle heat flow, radiogenic heat, heat conductivity and heat capacity of the sediments, as well as the fluid flow processes that transfer heat through the sediments (Lachenbrach, 1970). Therefore, conductive heat transfer was simulated with adequate boundary conditions and conductivity values that depend upon rock composition and porosity (Ungerer et al., 1990). Uniform radiogenic heat was assigned for each interval within the model, whereby the crust was initially set at 3.0 $\mu W/m^3$, and the sedimentary layers varied between 1.25 and 0.01 $\mu W/m^3$ (depending on the type of sediments - e.g., limestone: 0.62 $\mu W/m^3$; dolostone: 0.36 $\mu W/m^3$; shales and sands – 50%/50%: 1.25 $\mu W/m^3$; salt: 0.01 $\mu W/m^3$). This implies that a steady state vertical conduction is assumed per pre-defined sedimentary interval. The present-day basal heat flow input value was optimized by iteratively comparing calculated heat flow values and the known constrains (such as surface heat flow – Fig. 1, and Rock-Eval derived T_{max} – Table 2) through multiple simulations. Consequently, a constant heat flow value at the base of the crust of 40 mW/m^2 was set, resulting in the best fit with the published present-day surface heat flow values (Fig. 1) (Milivojević and Martinović, 2005; Milivojević, 1993; Miošić et al., 2010; Ravnik et al., 1995; Turrini et al., 2017) and the Rock-Eval derived T_{max} values determined in this study. The heat flow contribution from the lithospheric mantle is assumed not to vary during the evolution of the orogen, where the sedimentary part of the cross-section is modelled with higher details. Thermal/basin modelling resulted in estimating the geothermal gradient through space and time across the regional cross-section, leading to the assessment of the maturity of potential source rocks and their relationship with the prevailing tectonic evolution.

Potential source rocks have been identified in the field and sampled. In total, 15 samples were analysed at IFPEN by pyrolysis - Rock-Eval 6 (Espitalié et al., 1977) - to identify their kerogen types (derived from the oxygen index and hydrogen index ratio; van Krevelen, 1950), S2, TOC% and T_{max} values. Eight samples were proven to be potential source rocks of Triassic, Jurassic, Cretaceous, Eocene and Miocene ages (Table 2). Other TOC values and petroleum system characteristics have been taken from previous studies (Bega, 2015; Grandić et al., 2010; Mazzuca et al., 2015; Velić et al., 2015). Subsequently, calculated vitrinite reflectance values (EasyRo%) were derived from thermal modelling to estimate maturity levels. The calculation of vitrinite reflectance in TemisFlow™ is based on the EASY Ro% kinetics after (Sweeney and Burnham, 1990). The resulting EasyRo% values are immature from 0 to 0.55%, oil window from about 0.55–1.2%, gas window from 1.2 to 3.0%, and overmature when values are >3.0% (Teichmüller and Durand, 1983).

3.4. Geothermal energy assessment

Kinematic and thermal modelling provided reservoir property data (porosity and permeability values) as well as temperature values, which allowed for an initial assessment of the geothermal potential for the study-area in the Dinarides (e.g., temperature ranges and fluid flow characteristics of the target geothermal reservoirs). Calculated temperature, porosity, and permeability values were extracted from the constructed model for specific locations/depths along the studied cross-

Table 2
Input data derived from Rock-Eval pyrolysis on samples ($N = 15$) taken from the studied area. HK = High-Karst, D = Dalmatian, DF = Durmitor Flysch, UF=Ugar Flysch, VF = Vranduk Flysch, EBD = East Bosnian-Durmitor, M = Montenegro, B = Bosnia-and-Herzegovina, C = Croatia, L. Jurassic = Late Jurassic. S2 (mg/g), Tmax = Maximum temperature (in °C), TOC = Total Organic Carbon content (in %), HI = Hydrogen Index, OI = Oxygen Index (van Krevelen, 1950); I = oil prone (lacustrine), II = oil and gas prone (marine), III = gas prone (terrestrial), IV = none. ln(Estimated Ro) = (0.0078 Tmax) – 1.2 (Barker and Pawlewicz, 1986).

Serial #	Sample -ID	Age	Unit	S2(mg/g)	T_{max}	TOC	HI	OI	Kerogen	Estimated Ro%
1	Ec	Eocene	HK(M)	0.08	441	0.3	27	143	III	0.76 (oil-prone)
2	T2	Anisian	HK(M)	1.76	415	0.6	284	32	III	0.33 (immature)
3	T2	Anisian	EBD(M)	0.02	–	0.7	3	25	III	–
4	K2	Cretaceous	DF(M)	0.07	442	0.3	25	21	II/III	0.78 (oil-prone)
5	K2	Cretaceous	DF(M)	0.16	433	0.4	42	5	I/II	0.63 (oil-prone)
6	Ec	Eocene	HK(M)	0.01	–	0.3	3	83	III	–
7	Ec	Eocene	D(M)	0.72	442	0.9	80	49	III	0.78 (oil-prone)
8	K2	Cretaceous	DF(M)	0.02	–	0.2	10	95	III	–
9	K2	Cretaceous	UF(B)	0.01	–	0.1	7	114	III	–
10	K2	Cretaceous	UF(B)	0.04	434	0.2	17	143	III	0.65 (oil-prone)
11	J3	L. Jurassic	VF(B)	0.00	–	0.2	0	6	IV	–
12	T2	Anisian	EBD(B)	0.00	–	0.2	0	7	IV	–
13	J3	L. Jurassic	VF(B)	0.01	–	0.1	8	275	IV	–
14	J3	L. Jurassic	VF(B)	0.22	444	0.4	50	136	III	0.81 (oil-prone)
15	M	Miocene	HK(B)	–	435	2.9	579	41	I	0.66 (oil-prone)

section (Fig. 5). These values were used as input data for assessing the geothermal energy potential. The DoubletCalc software tool, developed by TNO Netherlands (https://www.nlog.nl/en/tools), was used to evaluate a hypothetical potential geothermal doublet lay-out in the study area and to evaluate related technical performance calculations. DoubletCalc is a semi-analytical performance assessment tool, which builds from a simple analytical formula the flow resistance in the targeted aquifer/reservoir. It is used to calculate the indicative power of a geothermal doublet and can generate probability graphs of potential geothermal prospects.

For the preliminary doublet layout, we assumed that the producer well is vertical, and the injector well is deviated with an angle of 45°. The outer diameter of the producer and injector wells are set to 6.125 in., and the doublet well distance at reservoir level is assumed to be 1000 m considering flow rates in the order of 216m^3/h (Milivojević, 1993). The skin factor of the producer is assumed 0. The skin factor of the injector is determined from the resulting penetration angle and horizontal drain length using the analytical formulations built in DoubletCalc, which results in a value of −2.81. The pumping pressure for the thermal loop is set to 65 bar. The properties of the aquifer/reservoir, wells and pumps, as well as producer and injector wells, which were used as input parameters for DoubleCalc simulations are presented in Table 3.

Table 3
Geotechnical input parameters for DoubletCalc simulations including properties for (A) aquifer/reservoir, (B) doublet and pump, as well as (C) producer and injector wells. Note that two scenarios were tested having the same input parameters except for aquifer gross thicknesses (scenario 1, between 800 and 1000 m; scenario 2 between 800 and 1800 m). Number of simulations per scenario is 1000.

A) Aquifer/ Reservoir	Min	Median	Max
Porosity (from Model)	9	17	25
Permeability (from Model)	0.07	76	151
net to gross (−)	0.4	0.5	0.6
gross thickness (m)	800	900 (Scenario 1) / 1500 (Scenario 2)	1000 (Scenario 1) / 1800 (Scenario 2)
top at producer (m TVD)	2610	2900	3190
top at injector (m TVD)	2520	2800	3080
water salinity	130,000	140,000	150,000
kh/kv ratio (anisotropy) (−)		1	
Surface temperature (°C)		14.6	
Geothermal gradient (°C/km)		20	

B) Doublet and pump	Value
Exit temperature heat exchanger (°C)	35
Distance wells at aquifer level (m)	1000
Pump system efficiency (−)	0.6
Production pump depth (m)	700
Pump pressure difference (bar)	65

C) Wells	Producer	Injector
Outer diameter (inch)	6.125	6.125
Skin producer (−)	0	0
Penetration angle (deg)	0	45
Skin due to penetration angle (−)	0.0	−1.34 (scenario 1) −1.45 (scenario 2)
Pipe segment sections (m AH)	3000	3700
Pipe segment depth (m AH)	3000	3000
Pipe segment inner diameter (inch)	6.125	6.125
Pipe segment roughness (milli-inch)	1.2	1.2

4. Results

4.1. Offshore seismic interpretation

Seven key horizons (R1, oldest, to R7, seabed) and several faults were identified on the interpreted 2D seismic section (Fig. 5a). These horizons and their associated stratigraphic packages (S1 to S7, respectively) were traced based on amplitude reflection characteristics, as well as the reflectors contacts and terminations patterns. This representative seismic profile illustrates clear geometries that are related distinctly to two domains: the South Adriatic basin (to the SW) with overall relatively flat stacking of reflectors, and the Apulian-Dalmatian domain (to the NE) with deformed reflectors and interpreted major thrust faults.

4.1.1. Triassic-Jurassic syn- and post-rift phases

The deepest horizon (R1) is characterized by high amplitude, subparallel, discontinuous reflectors, and is cross-cut and vertically displaced by numerous normal faults (Fig. 5a). Because it is offset by such normal faults forming horst and graben structures, typical features ascribed to the Middle Triassic – Early Jurassic rifting, R1 is interpreted to represent the Late Triassic. It overlies an overall moderate to high amplitude, sub-parallel to chaotic reflection package (S1) that could represent the Paleozoic - Triassic mixed sequence of carbonates and clastics. In the duplicated series in the Apulian-Dalmatian domain, R1 horizon is likely to be underlain by Permo-Triassic evaporites and salt. The overlying Late Jurassic horizon (R2) postdates the rifting and formation of the Middle Triassic - Early Jurassic normal faults ascribed to the rifting event. R2 is characterized by low to moderate amplitude subparallel reflectors, overlying a seismic interval showing, generally, low amplitude, subparallel to chaotic, discontinuous reflectors (S2) that fits with *syn*-rift sedimentary sequences with shallow carbonate facies on the top of horst structures and deeper marine facies in the graben structures. This is characterized by generally parallel (though discontinuous) reflectors in the South Adriatic basin and inclined higher-amplitude reflectors, that are typical of carbonate ramp build-ups, in the northeastern margin of the Adriatic basin domain and in the Apulian-Dalmatian domain (i.e., above the large horst structure, Fig. 5a). Like the underlying R1 horizon, R2 is offset by a thrust fault representing the transition from the Adriatic basin to the Apulian-Dalmatian carbonate platform.

4.1.2. Eocene-Oligocene shortening

R3 horizon consists of high amplitude, relatively parallel and continuous, condensed reflectors (especially in the SW part of the profile; Fig. 5a). It overlies a seismic interval (S3), which, in the South Adriatic basin, is made up of a relatively thin (<0.5 s. TWT) package of low to moderate amplitude, parallel reflectors. Whereas, in the centre of the profile towards the NE, the thickness of S3 exceeds 1.5 s TWT, featuring, sub-parallel and inclined reflectors with relatively stronger amplitudes. Therefore, R3 horizon is likely to represent the top of the Cretaceous-Paleocene platform carbonates, associated to a major unconformity (U1) – which is further confirmed by the observed onlapping reflectors of the overlying S4 package. The seismo-stratigraphic characteristics of the S4 package (i.e., discontinuous, sub-parallel, downlapping reflectors) invoke thick intervals of sand, silt, clay, marls and turbidites, known to have filled the South Adriatic basin through the Eocene and Oligocene times (Figs. 4a and 5b). This observation infers a top Oligocene age to the overlying horizon (R4) which displays a major high amplitude sub-parallel reflector (Fig. 5a). The thickness variations of S4 indicate that the sediments are likely derived from the NE of the South Adriatic basin and were deposited in the basin as prograding deltaic deposits. Thrusting within the Dalmatian unit was active during the Eocene – Oligocene contraction, which uplifted the R4 horizon in the hanging-wall (Fig. 5b). The prevailing increased thickness of S4 at the

contact with the thrust front suggests that this package represents a *syn*-kinematic sequence corresponding to the Eocene - Oligocene phase of contraction. The uplift of the Apulian-Dalmatian zone resulted in the erosion of the S4 sediments, further affected by the renewed post-middle Miocene thrusting (Fig. 5a).

4.1.3. Miocene-Pliocene contraction phases

R5 horizon is characterized by moderate to high amplitude sub-parallel reflectors in the South Adriatic basin and moderate to low amplitude reflectors in the Apulian-Dalmatian zone (Fig. 5a). A seismic reflection-free pattern is observed along this horizon, which may represent a thin salt layer deposited during the Messinian Salinity Crisis (MSC) of the Mediterranean, known to be absent or to have reduced thicknesses in the Adriatic domain (Haq et al., 2020). Channel geometries observed in S5 package in the South Adriatic basin can be associated with the known Miocene fluvial type of sediment deposition. R5 is interpreted as the upper limit of the Miocene, which coincides with a major unconformity observed in the Apulian-Dalmatian domain (U2, Fig. 5a). The overlying Zanclean sediments show a low amplitude prograding wedge with channels and wedge shape morphologies observed in the S6 package, indicating fluvial and deltaic type of sedimentation. S6 shows the typical Zanclean foresets that formed after the MSC, as they directly overlie the Messinian unconformity (Clauzon, 1990; Gorini et al., 2005). This deposition was subsequently affected by renewed thrusting, observed in this seismic line in the S6 and S7 (Pliocene – Quaternary) packages. A major antiform above the frontal thrust faults is associated to this thrusting uplift. The alternating low to moderate amplitude parallel reflectors of S6 can represent clastic turbidite deposits, which were triggered during the thrust activation associated with slope instability. These faults must have remained active in the Pliocene, suggesting that S6 package represents – at least partially – a syn-kinematic sequence (Fig. 5a). The R7 horizon represents the seabed, overlying relatively low amplitude, parallel, continuous reflectors – typical of under-compacted deeper marine shale deposits (S7). This S7 package reflectors onlap onto the R6 horizon above the thrust faults in the Apulian-Dalmatian carbonate platform domain.

4.2. Kinematic restoration modelling results

The integrated regional cross-section, including the interpreted 2D

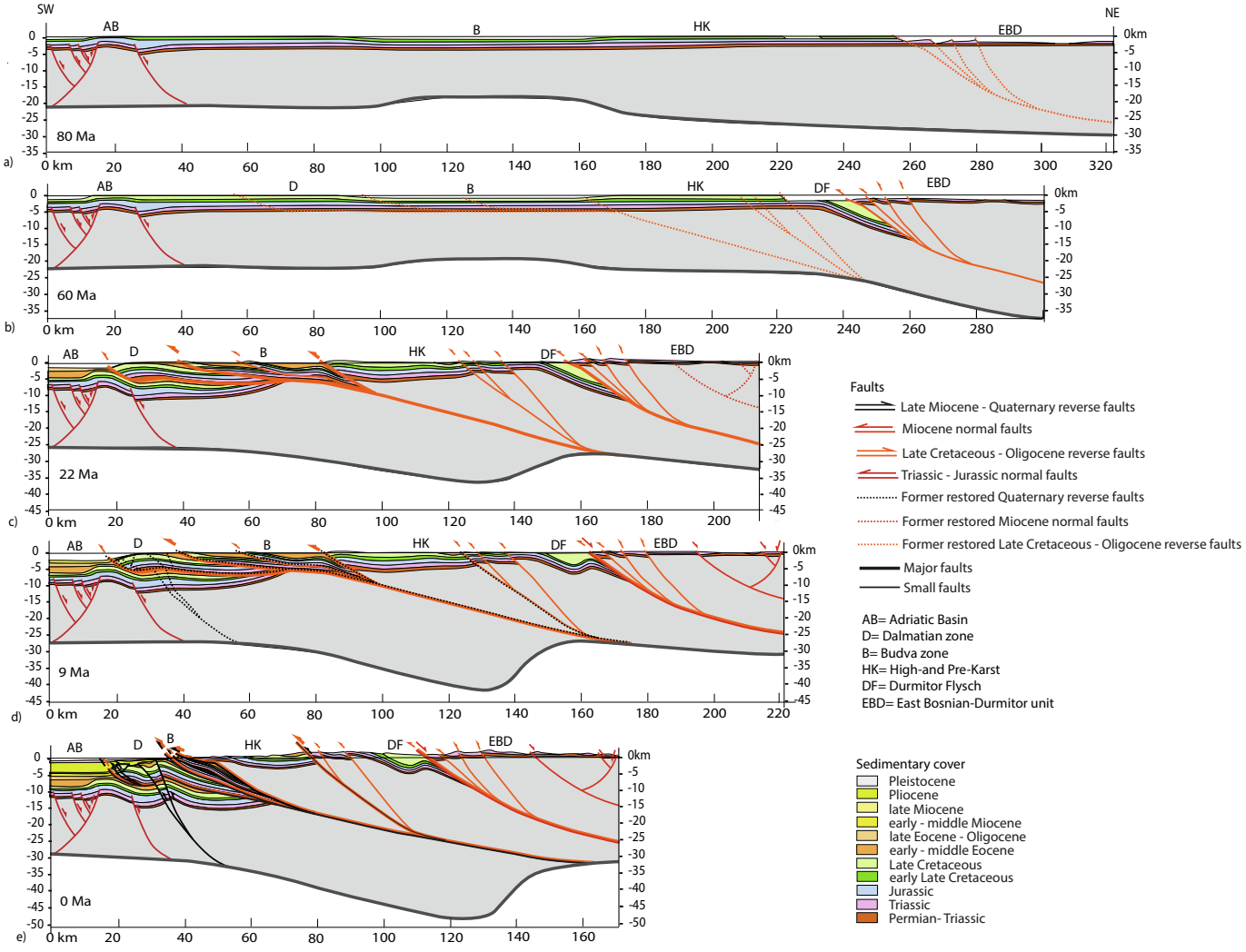

Fig. 6. Kinematic evolution of the along the Dinarides section (AB = South Adriatic basin, D = Dalmatian unit, B = Budva unit, HK = High-Karst unit, EBD = East Bosnian-Durmitor unit, DF = Durmitor Flysch): a) Late Triassic – Early Jurassic formation of the Adriatic basin due to rifting and associated horst and-graben structures, then carbonate platform build-up took place until Late Cretaceous times; b) Late Cretaceous period of contraction resulted in the SW-ward thrusting of the East Bosnian-Durmitor unit over the Durmitor Flysch; c) until Oligocene the gradual migration of contractional deformation towards the orogenic foreland could be associated with southwestward nappe stacking of the High-Karst, Budva and Dalmatian units; d) Miocene extension resulted in the footwall exhumation of the East Bosnian-Durmitor – Durmitor Flysch contact; and e) since the latest Miocene times contraction induced high-angle reverse faulting and reactivated former structures and nappe contacts in the Dinarides.

seismic reflection offshore profile (Fig. 5a) and the onshore segment, is displayed in Fig. 5b. The restoration of this cross-section, performed with the KronosFlow™ (OpenFlow Suite™), is illustrated by five time-steps spanning the Late Cretaceous to present day (Fig. 6). Most of the shortening in the internal parts of the Dinarides took place during latest Cretaceous, characterized by the SW-ward thrusting of the East-Bosnian Durmitor over the High-Karst and Pre-Karst units over a minimum ~20 km, besides the observed ~2 km internal East Bosnian-Durmitor unit shortening (Fig. 6b). The footwall was buried to depths in the order of 12 km.

The Eocene - Oligocene shortening created a SW-vergent low-angle thrusting in the external Dinarides, with a gradual migration towards the foreland (Fig. 6c). The High-Karst over Budva thrust accommodates ~10 km of shortening, associated with the ~3 km exhumation of the High-Karst unit. Furthermore, ~10 km of internal shortening took place within the Budva unit. The Budva over Dalmatian thrust accommodates a minimum of ~17 km of shortening (Fig. 6c). The Budva thrusting can be associated with ~3 km exhumation. ~48 km thrusting took place at the contact between the Dalmatian unit and the Adriatic basin, which created the space for the deposition of up to 4 km of syn-kinematic sediments. The Dalmatian thrusting also resulted in the erosion of >1 km of sediments in its hanging-wall. The total amount of Eocene – Oligocene shortening is ~85 km (Fig. 6c).

The Early – Middle Miocene extension reactivated the East-Bosnian Durmitor – High-Karst and Pre-Karst contact, associated with asymmetric uplift of ~6 km in its footwall (Fig. 6d). The minimum amount of horizontal extension is in the order of 8 km at this contact. The renewed post-Middle Miocene contraction resulted in the formation of high-angle N- and S-vergent reverse faults and the reactivation of former thrust contacts, with significant effects in the external-most part of the orogen. The thrusting of the High-Karst over Budva resulted in ~12 km of shortening, associated with the erosion of ~3 km of Jurassic to Cretaceous sediments in its hanging-wall and further burial of the Budva unit to depths of ~17 km. About 3 km of internal shortening have been measured in the central part of the High-Karst unit (Fig. 6e). The internal thrusting that took place between the sub-units of the larger Budva zone accommodates a minimum of ~15 km of shortening, associated with the erosion of ~2 km of Triassic to Eocene sediments. The thrusting of the Budva unit over the Dalmatian unit accommodated about 13 km of shortening, associated with the erosion of ~1 km of Eocene sediments in the Dalmatian unit. Internal shortening of about 5 km is measured inside the Dalmatian unit, associated with transpressional structures that are offset by high-angle thick-skinned reverse and/or strike-slip faults (Fig. 6e). The Dalmatian overthrusting can be associated with the erosion of hundreds of metres of Miocene and Pliocene siliciclastic sediments inside the Dalmatian unit. Therefore, the minimum total amount of shortening accommodated from the Late Miocene - Quaternary is ~53 km (Fig. 6e).

4.3. Geochemical analyses of principal potential source rocks

Rock-Eval pyrolysis was achieved on 15 representative rock samples which were collected from key surface-exposed sites along the investigated cross-section (Fig. 5b). These samples represent the three known principal potential source rocks (Triassic, Late Cretaceous - Paleocene, and Eocene - Oligocene; Fig. 4). Table 2 summarized the related geochemical analyses results in terms of S2, T_{max}, TOC, HI, OI, type of Kerogen as well as estimated Ro% (from T_{max}, see Methodology, above). Most of the analysed samples revealed the local thermal evolution of the host-rocks and resulted in interpreted Kerogen types II and III with very low TOC values (<1%).

4.4. Thermal (basin) modelling results

The 2D thermal/basin model of the restored cross-section is essential for evaluating the potential petroleum systems (expulsion, migration and trapping of hydrocarbons) as well as the geothermal energy potential. By coupling the restored cross-section model (KronosFlow™) with the basin/thermal model (TemisFlow™) via the common platform OpenFlow Suite™, the structural model with backstripped geometries was used as input data for simulating the thermal evolution. Results of this coupled modelling approach revealed a generalized pattern of heat flow variations that are associated with crustal deformation while highlighting the heat flow and temperature distributions in the various tectonic units and in the proximity of major faults (Fig. 7a). Furthermore, the major thrust faults, whether duplicating series in thin-skinned geometries or deeply rooted in the Moho showed a significant impact not only on the facies distributions and architecture but also on the thermal distribution and deduced fluid flow. The resulting heat flow distribution is based on constant heat flow input values at the base of the Moho and the calculated heat flow across the investigated section (up to 80 mW/m^2; Fig. 7a). During episodes of thrusting, the hanging-walls and upper parts of the footwalls in various tectonic units show increased conductivity and heat flow, whereas the deepest parts of the footwalls show lower heat flow as the result of compaction and lower conductivity. The processes of heat transfer along faults and in the specific tectonic units across the orogen have been integrated in the achieved coupled model, leading to better assessment of potential geo-resources.

Calculated heat flow and temperature values were locally extracted from the coupled model to assess the thermal conditions for viable geothermal energy and petroleum systems prospects in specific locations. The evolutions of geothermal gradients in each tectonic unit were derived from the model to characterize larger areas, at the scale of tectonic units (Fig. 7b). During the Triassic – Early Jurassic rifting the estimated geothermal gradient increases from 17 °C/km to about 22 °C/km in the Budva unit compared to 19 °C/km in the adjacent areas. Until Late Cretaceous times the calculated geothermal gradient had an approximate continuous value of 20 °C/km on average across the orogen. After the Cretaceous - Eocene thrusting the deduced geothermal gradient was 14 °C/km in the Budva unit, 20 °C/km in the South Adriatic basin and 16 °C/km in the High-Karst unit. After the Miocene extension the geothermal gradient was about 25 °C/km in the Bosnian-Durmitor Flysch, 18 °C/km in the Budva unit, and 26 °C/km in the Dalmatian and South Adriatic basin. At present-day the geothermal gradient in the Budva unit, Dalmatian unit and South Adriatic basin is 19 °C/km, in the High-Karst unit 18 °C/km and in the Bosnian-Durmitor Flysch 20 °C/km (Fig. 7b). The model also allows to extract the evolution of calculated temperature (Fig. 7c), and vitrinite reflectance (Fig. 7d) with depth and time from any cell.

4.5. Preliminary evaluation of geothermal energy potential

The Cretaceous and Triassic carbonates, that are characterized by high permeability, are considered as the main targets for geothermal energy development in the study area. These potential reservoirs occur along the investigated cross-section of the Dinarides within approximate depths of 3000 m, underlying sealing layers and structures. The thermal model yielded first estimates of the temperatures of the Cretaceous and the deeper Triassic carbonates in the potentially prospective areas of the Dalmatian, High-Karst and Durmitor Flysch units.

First, the thermal model was used to locally extract temperature values of the target reservoirs (at present-day depth) in the prospective areas. These values were further used to confirm the calculated geothermal gradients at the larger regional scales. Then, the temperatures at depth of the target reservoirs in the Dalmatian, High-Karst and Durmitor-Flysch units, were estimated by adding an average mean annual air (surface) temperature of 14.6 °C (Bonacci, 2017) to the calculated subsurface temperature values that are based on the local geothermal gradients. In the Dalmatian area, the Cretaceous reservoirs can be reached at about 3000 m with estimated temperatures exceeding 75 °C (Location 1; [L1], Fig. 5b). In the High-Karst area, the Cretaceous reservoir is shallow with depths of up to 1500 m reaching temperatures

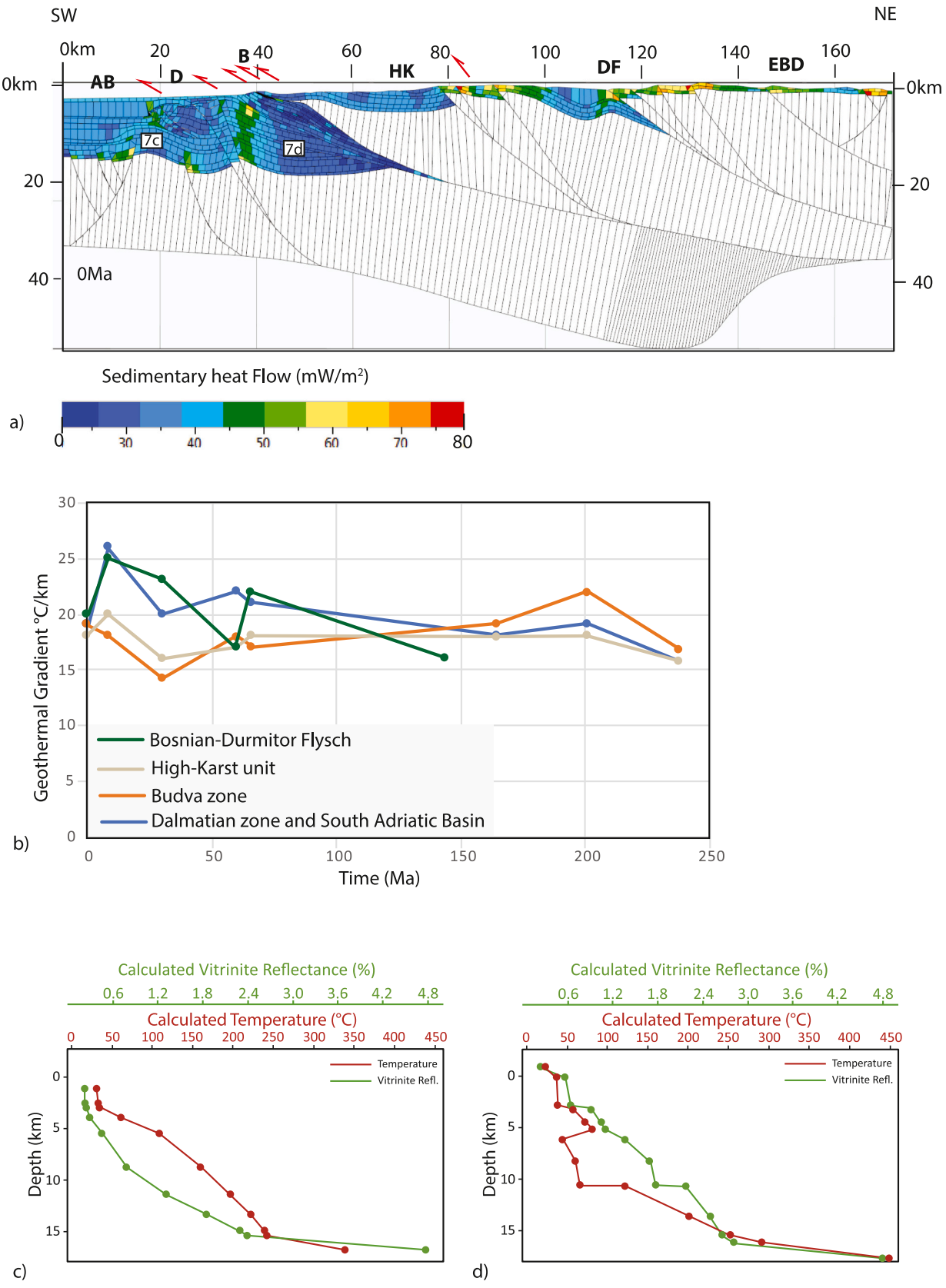

Fig. 7. a) Basal heat flow distribution across the sedimentary cover of the present-day Dinarides section, reflecting the constant basal input heat flow value of 40 mW/m^2. This corresponds with the present-day surface heat flow values; b) Diagram demonstrating the variable geothermal gradients across the Dinarides through space and time, which were extracted from the thermal model; c, d) Temperature (°C) and vitrinite reflectance (%) depth-evolution plots extracted from the thermal model, from two subsurface locations (indicated in Fig. 7a).

of about 45 °C, which are likely insufficient for a geothermal doublet to be economically feasible. The Triassic limestones and dolomites in the High-Karst unit are around 3000 m deep (Location 2; [L2], Fig. 5b) where temperatures could exceed 75 °C, which is sufficient for low temperature geothermal energy production. In the Durmitor Flysch, both Cretaceous and Triassic reservoirs are found at depths not exceeding 3000 m with temperatures reaching 75 °C (Location 3; [L3], Fig. 5b). The minimum, median and maximum values of porosity and permeability (input data for DoubletCalc simulations) have been derived from the TemisFlow™ model for the relevant depth interval and sediments of the target reservoirs (Table 3).

A heat pump system was incorporated in the DoubletCalc simulations to increase the production temperature from the geothermal source (by the condenser), and to decrease the return temperature (by the expansion valve) so that the heat delivery from the geothermal source can be increased. Henceforth, reservoir temperatures are raised about 15 °C to reach a total value of 90 °C at the district heating network output side of the heat pump. The heat pump lowers the exit temperature of the geothermal fluid after the heat exchanger to about 35 °C (Table 3).

Two different scenarios of potential geothermal doublet were evaluated, based on median thicknesses of 900 m and 1500 m for depths of 3000 m (Table 4). The first scenario is applicable to the Triassic carbonates, whereby the DoubletCalc results in terms of P50 and P10 values of geothermal power are around 10.07 and 12.0 MW_{th} respectively (Fig. 8). The second scenario (median thickness of 1500 m), is applicable to the Cretaceous carbonates, resulting in higher P50 and P10 values of geothermal power of approximately 13.01 and 15.34 MW_{th}, respectively (Fig. 8).

5. Discussion

5.1. Implications of kinematic modelling for quantifying thick- and thin-skinned deformations

The Late Cretaceous phase of contraction affected mostly the internal part of the Dinarides. The latest Cretaceous thrusting of the East Bosnian-Durmitor over the High-Karst and Pre-Karst units has a calculated shortening rate of ~0.9 mm/yr (80–60 Ma, Fig. 6a-b). This thrusting is associated with footwall foredeep sedimentation rates of ~0.1 mm/yr, burying the *syn*-kinematic turbidites (Durmitor Flysch) to an estimated depth of ~12 km at a rate of ~0.6 mm/yr, based on the kinematic modelling. The Eocene – Oligocene phase of contraction (average shortening rate of ~2.2 mm/yr) affected the external-most parts of the Dinarides (Budva and Dalmatian units, Fig. 6a-c). The largest amounts of shortening were accommodated by the thrusting of the Dalmatian unit over the Adriatic foreland with rates of ~1.3 mm/yr. The reconstructed kinematic evolution across the Dinarides is, henceforth, differentiated between a thick-skinned geometry in the High-Karst and more internal parts of the orogen and a thin-skinned geometry in the Budva and Dalmatian units.

The thin-skinned part can be associated with subthrust structures like the ones inferred by Bega (2015) in offshore Montenegro, and the ones observed in the Cukali zone of Albania (Velaj, 2015). Thrusting led to anticlinal geometries with large wavelengths during the uplift of the Dalmatian unit (Fig. 6c), typical of the Dinaric phase of contraction. The exhumation of the Dalmatian unit resulted in the erosion of Eocene sediments (Fig. 3). This large-scale thrusting was likely responsible for the ~4 km of basin subsidence, associated with the formation of the foredeep wedge in the Adriatic foreland (see also Bega, 2015). The 4 km thick sequence of Eocene to Oligocene syn-kinematic siliciclastics was coevally deposited in this basin, characterized by onlapping over the carbonate ramp bounding the South Adriatic basin (Fig. 5a, syn-kinematic sequence 1). The calculated 48 km of shortening accommodated by the frontal thrust of the Dalmatian unit over Adriatic basin cumulates the effects of both the Eocene – Oligocene and post – Middle Miocene thrusting. Note that available seismic data does not allow a correct differentiation at depth of the kinematic mechanism of the two internal-most thrusts, although their offsets are rather clear (Fig. 5a). There are two possible interpretations. These thrusts could be thick-skinned and represent the continuation of an *E*-W oriented mid-Adriatic lineament in the offshore Montenegro, as previously speculatively inferred (Fig. 5b, see also Bega, 2015). Alternatively, they could be thin-skinned and root in Permo-Triassic salt, observed to have higher thicknesses in the offshore Adriatic and more internal units in the NW Dinarides (Fig. 5c).

The Early-Middle Miocene extension reached deformation rates higher than 0.8 mm/yr. The East Bosnian-Durmitor thrust was reactivated as a normal fault detachment, where its Pre-Karst footwall was exhumed with 6 km at rates ~0.5 mm/yr (Fig. 6c-d). The erosional unconformity at the base of the Durmitor Flysch has an isostatic rebound geometry typical for an extensional detachment, associated with the Moho uplift and mantle upwelling. From the total amount of post-middle Miocene shortening (minimum of 53 km), an overall shortening rate of about ~5.9 mm/yr can be estimated, which is in close approximation to the velocities of the Adriatic indentation that has been investigated during previous GPS studies (Bennett et al., 2008; Grenerczy et al., 2005).

Within the restored present-day interpretation, the thin-skinned structures of the Dalmatian unit are truncated by basement-involved reverse faults, invoking thick-skinned deformation in the Adriatic foreland during the Neogene. These faults show transpressional structures with high inclinations and have been interpreted to be of Late Pliocene – Quaternary age, which is indicated by the wedge structure above the active Dalmatian – Adriatic basin thrust that is filled with Pliocene sediments (Fig. 3). The high-angle faults can be associated with the

Table 4
Geotechnical output parameters for DoubletCalc simulations at mid-aquifer depth for scenarios 1 and 2. The Monte Carlo cases stochastic input values are shown as well as the Base Case median value input values for both scenarios 1 and 2.

	SCENARIO 1				SCENARIO 2			
Monte Carlo cases (stochastic inputs)	P90	P50	P10	Base case	P90	P50	P10	Base case
Aquifer kH net (transmissivity) (Dm)	15.17	34.04	53.32	34.2	23.82	52.29	87.76	57.0
Mass flow (kg/s)	41.66	63.7	72.96	63.68	54.94	73.25	81.6	74.95
Pump volume flow (m^3/h)	139.0	213.3	244.2	213.0	184.3	245.8	274.2	251.5
Pump power (kW)	418.2	642.0	734.9	641.1	554.5	739.7	825.2	756.9
Geothermal power (MW)	6.38	10.07	12.0	10.19	9.42	13.01	15.34	13.62
COP (kW/kW)	14.6	15.8	17.0	15.9	16.2	18.8	19.1	18.0
Aquifer pressure at producer (bar)	290.93	308.76	326.8	308.72	290.87	308.87	326.86	308.72
Aquifer pressure at injector (bar)	292.11	308.86	325.25	308.72	292.2	308.53	325.67	308.72
Pressure difference at producer (bar)	11.76	15.99	24.03	16.01	7.93	12.1	20.08	11.31
Pressure difference at injector (bar)	16.25	22.22	32.65	22.16	10.93	16.56	27.13	15.46
Aquifer temperature at producer* (°C)	78.43	81.58	84.86	81.6	82.66	87.06	90.95	87.6
Temperature at heat exchanger (°C)	76.07	79.4	82.73	79.67	80.58	85.01	88.82	85.7
Pressure at heat exchanger				25.67				25.86

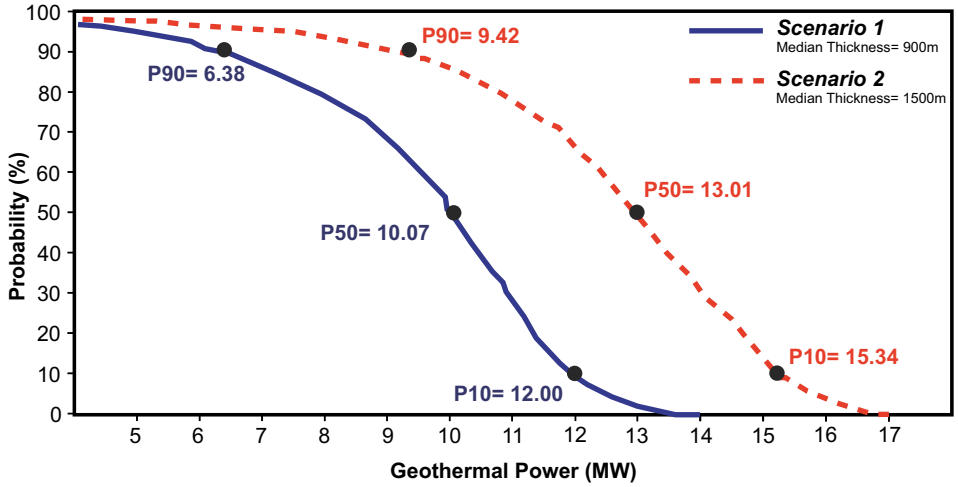

Fig. 8. Results of DoubletCalc calculations illustrated as a diagram showing the geothermal power (MW) and probability (%) for 900 m thick Triassic carbonates (Scenario 1) and 1500 m thick Cretaceous carbonates (Scenario 2) reservoirs/aquifers, in the Dalmatian, High-Karst, and Durmitor Flysch zones.

formation of transpressional folds in the Dalmatian unit, and have a deep-seated basement involved structure. These faults may also be pathways for deep-seated hydrothermal fluids and hydrocarbon migration. Thus, the interpreted evolved thin-skinned structures during the Eocene – Oligocene pre-dates a later Neogene phase of contraction that induced such thick-skinned high-angle reverse faults. The Middle Adriatic ridge, situated in the Adriatic Sea, has an E-W oriented transpressive structure that spreads along many branches (Scisciani and Calamita, 2009). One of these branches prolongs to and affects the sub-thrust structure in offshore Montenegro (see also Bega, 2015), which is demonstrated by the high inclined reverse faults (Fig. 5). The timing of activity of these high-angle reverse faults is interpreted to be during Paleogene - Miocene and Late Pliocene – Quaternary times, but a higher resolution of this timing remains speculative (Scisciani and Calamita, 2009). Therefore, different scenarios for the superposition relationship between the external sub-thrusts and the high-angle reverse faults could be made (van Unen et al., 2019a, 2019b). Furthermore, the uplift of the Dalmatian unit, likely resulted in the erosion of the Miocene sediments creating unconformities, such as the U2 unconformity that is indicated in Fig. 5a. During Late Miocene – Quaternary times a second period of large *syn*-kinematic siliciclastic deposition took place (Fig. 5a, syn-kinematic sequence 2), which can be associated with the main episode of the foredeep wedge formation in the Adriatic basin (Picha, 2002).

The thick syn-kinematic sequence 2 overlies the top Messinian unconformity in the Adriatic basin (Fig. 5a). The basin subsidence of ~4 km (with rates of ~0.8 mm/yr) underwent simultaneous infill of 4 km of Late Miocene to Pleistocene sediments. The lower shortening rates of 0.6 mm/yr of the Dalmatian unit over the Adriatic basin indicates a low impact of orogenic loading, and hence less likely the cause of the observed strong basin subsidence. Therefore, lithosphere flexure due to subduction could have resulted, most probably, in the observed strong flexural subsidence (Wortel and Spakman, 1992; Zoetemeijer et al., 1993). This can be related to the indenting Adriatic plate (Picha, 2002; Grenerczy et al., 2005; van Unen et al., 2019a, 2019b). A similar flexure of the Adriatic lithosphere has been indicated beneath the Apennine foreland, which is responsible for the formation of the Apennine foredeep basin (Bertotti et al., 2001; Royden, 1993). Strong flexural subsidence associated with rapid infill might have resulted in optimal conditions for the accumulation and preservation of microbial gas-prone source rocks.

5.2. *Implications of kinematic and thermal modelling for assessing potential geothermal energy resources*

Results of the kinematic/thermal models as well as collected data and produced calculations were used to get a first indication on the geothermal potential in the study area. Based on porosity and permeability as well as temperature values derived from thermal modelling, potential geothermal reservoirs could be assigned to the high permeable Triassic limestones and Cretaceous carbonates mainly in the eastern part of the studied section. To determine a suitable area for geothermal exploration a sealing layer must be present above the high potential water reservoir.

The permeable Cretaceous carbonates (about 2 km thick) that are present in the Dalmatian unit and sealed by the Oligocene and Neogene siliciclastics could serve as potential geothermal reservoirs as they reach depths of 3 km. With the temperature gradient of 19 °C/km, temperatures exceeding 72 °C can be reached at such depths, indicating good potential for low temperature geothermal exploration.

Within the High-Karst unit most of the permeable Cretaceous carbonate strata crop-out at the surface, therefore the temperatures of the reservoir water are not sufficiently high for geothermal energy production. The underlying 1 km thick Triassic limestones reach depths of about 3–4 km. With the temperature gradient of 18 °C/km, temperatures of about 69 °C can be reached at 3 km depth, indicating a good potential for low temperature geothermal exploration. The sealing intervals above these potential reservoirs might be insufficient as demonstrated in the cross-sections and produced models, which makes the geothermal potential within these areas low.

In the Durmitor Flysch area, the Triassic carbonates reach sufficient depths (~3 km) and thicknesses (up to 1 km) and are overlain by the Ugar and Vranduk Flysch and bounded by fault structures. The latter may provide good sealing potential depending on the permeability of the faults. With the temperature gradient of 20 °C/km, temperatures of 75 °C can be reached at 3 km depth, indicating the best potential for geothermal exploration, compared to the other southwestern areas. The DoubletCalc calculations (Fig. 8) were based on the thermal modelling results across these areas. Two values for the thickness of the reservoir/aquifer were considered (scenario 1: 900 m; and scenario 2: 1500 m; Table 3, Fig. 8). These calculations confirmed that an increased thickness of the aquifer will also increase the probability of success of a potential geothermal doublet (calculated P50 geothermal power of 10.07 MW_{th} and 13.01 MW_{th} for scenario 1 and scenario 2, respectively).

The predicted geothermal power production is characterized by a threshold value, on which the potential business case is based. For

example, this threshold value is critical for covering the costs of geothermal exploration drilling by an insurance fund. For developing a viable business case, the threshold power should be financially underpinned by proprietary cash flow calculations and underlying constraints. Hence, the drilling costs of different doublet designs should be considered (e.g., sub-horizontal wells are usually more expensive than vertical or less deviated wells). A good probability of success is often associated with a probability exceeding 50% of producing >10 MW_{th} (van Wees et al., 2012). Our first estimates for geothermal energy production from Triassic and Cretaceous reservoirs in the study area, meet this requirement (P50 > 10 MW_{th}) and could therefore yield positive business cases, while taking note that the proposed doublet design remains conceptual, and the calculated values are indicative. In this study, the penetration angle of the injector is assumed to be 45° and the producer is assumed to be vertical, whereas a sub-horizontal well design would, alternatively, increase the power potential of the doublet by optimizing the drainage length through the intruded formation. Additional work is needed in terms of reservoir quantitative characterization, geothermal doublet design and cost estimation, doublet behaviour modelling, as well as economics and optimized engineering parameters for local circumstances. These studies could improve the predicted power values and lead to successful and sustainable exploitation of the geothermal energy in the Dinarides.

5.3. Analysis of source rocks and maturity modelling

The three major source rocks – i.e., organic-rich intervals capable of generating hydrocarbon – (of Triassic, Late Cretaceous - Paleocene, and Eocene – Oligocene ages; Fig. 4) were investigated in terms of maturation degrees derived from the thermal model and confirmed by geochemical analyses on representative samples (Table 2). The Triassic source rocks along the whole cross-section reached the oil window by Late Cretaceous times, because of sufficient burial during the deposition of the thick sequence of platform carbonates (Fig. 9a). Within the Dalmatian unit, where these Triassic source rocks were deposited in downthrown syn-rift blocks, they reached both the oil and gas window (Fig. 9a). Geochemical analyses of samples of Triassic source rocks (from outcrops, this study) showed that they represent types II and III kerogens with residual TOC values of 0.7% (Table 2), and calculated vitrinite reflectance values between 0.55 and 1.69 Ro%, representative for the oil and gas windows.

During the latest Cretaceous – Eocene phase of contraction, the footwall of the East Bosnian Durmitor – Bosnian-Durmitor Flysch contact was deeply buried (about 10 km). This resulted in increasing the

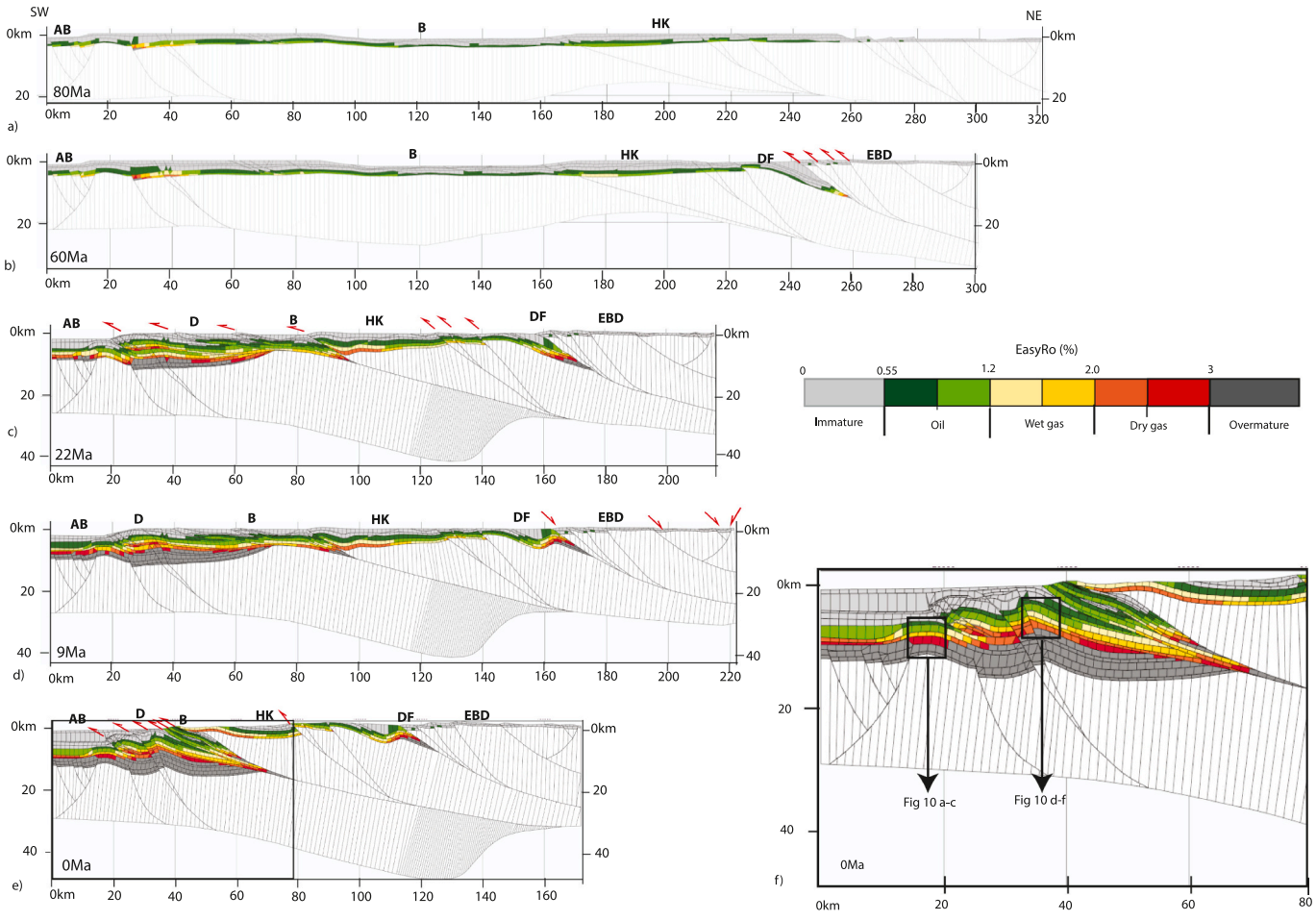

Fig. 9. Thermal Maturity evolution of the restored Dinarides section: a) Maturation of Middle Triassic source rocks began after sufficient burial was reached during the deposition of the thick carbonate platform across the entire orogen; b) The thrusting of the East Bosnian- Durmitor over the Durmitor Flysch during Late Cretaceous resulted in the burial and the maturation of the Triassic shales and Durmitor Flysch in the footwall of the thrust contact; c) During the Eocene – Oligocene thrusting and sedimentation, Triassic and Cretaceous source rocks became mature all across the area; d) The exhumation of the Durmitor Flysch unit during the early - middle Miocene extension, caused the mature Durmitor Flysch to reach the surface. Simultaneously, the rapid and thick sedimentation in the Adriatic basin resulted in the maturation of Eocene - Oligocene source rocks; e) Continued thrusting, the reactivation of former thrust and thick sedimentation in the foreland from Late Miocene onwards resulted in increased burial of the footwall areas and an increase in maturation of Middle Triassic, Cretaceous and Eocene - Oligocene source rocks in the Budva unit, Dalmatian unit and South Adriatic basin; f) Zoom-in of the foreland-area of e), which shows the location of the areas described in Fig. 10.

maturity of the Triassic source rocks, reaching the oil and gas windows (Fig. 9b). The calculated range in vitrinite reflectance of the Triassic source rocks in the footwall of this thrust contact is between 0.55 and 1.82 Ro% (representative of oil and gas window).

The Eocene - Oligocene foreland-ward migration of thrusting is associated with the burial of the Budva and Dalmatian units, which resulted in further maturation of source rocks in these units (Fig. 9c). Within the Budva unit Triassic source rocks reached the oil and gas windows with calculated vitrinite reflectance values between 0.67 and 1.8 Ro%. Within the Dalmatian unit, the Triassic source rocks reached the oil and wet gas windows with calculated vitrinite reflectance values between 1.1 and 1.5 Ro%, while the Cretaceous source rocks reached the oil window with calculated vitrinite reflectance values between 0.55 and 0.82 Ro%. The Triassic source rocks are overmature within the Adriatic foreland, based on simulation results. Cretaceous source rocks reached the oil window in the SW-part and gas window in the NE-part beneath the Dalmatian unit (Fig. 9c). These Cretaceous source rocks have vitrinite reflectance values between 0.69 and 2.12 Ro%. Below the Dalmatian thrust within the Adriatic foreland, Eocene - Oligocene source rocks reached the oil and gas window with calculated vitrinite reflectance values between 0.55 and 1.53 Ro%.

The Eocene – Oligocene source rocks in the southwestern-most part of the Adriatic foreland reached the oil window as a result of the Oligocene – Miocene sedimentation and the subsiding Adriatic foreland. These source rocks have calculated vitrinite reflectance values between 0.6 and 1.1 Ro%. Beneath the Dalmatian thrust, more to the NE, they reached the gas window with values of up to 2.4 Ro% (Fig. 9d). Continued thrusting and the reactivation of the High-Karst – Budva and Budva – Dalmatian contacts from latest Miocene times onwards can be associated with an increase in burial of the footwall areas (Fig. 9e,f). During this time, Triassic source rocks reached the oil and gas window in the Budva unit. These source rocks have calculated vitrinite reflectance values between 0.89 and 2.4 Ro%. Cretaceous source rocks in the Budva unit reached the oil window, which have calculated vitrinite reflectance values between 0.55 and 0.94 Ro%. Within the Dalmatian unit, the Eocene – Oligocene source rocks reached the oil window in the immediate footwall of the Budva contact, which have calculated vitrinite reflectance values between 0.55 and 0.71 Ro%. The mature Eocene source rocks in the Dalmatian unit can be associated with type III kerogens and TOC values of up to 0.9% (Table 2).

5.4. Implications of kinematic and thermal modelling for assessing potential petroleum systems

The constructed 2D model is subdivided in three distinct structural domains with respect to the petroleum systems (i.e., Adriatic basin, Dalmatian zone and onshore Dinarides). As the structures and internal sedimentary intervals of the cross-section were built mainly from surface kinematic analyses, the deeper sedimentary structures for the onshore part of the cross-section remain speculative with under-estimated petroleum potential. Yet, present-day observed seeps at the surface and in well logs confirm active petroleum systems in the studied area. For the offshore part, pertinent constraints based on available seismic reflection data led to a better assessment. Modelling was used to estimate through the calculated thermal distribution and source rock intervals the potential maturity and henceforth degree of expulsion of hydrocarbon during the tectonic evolution across these domains. The analysed source rocks, though limited in this study, help as well to constrain and calibrate the proposed models.

5.4.1. Adriatic basin

Three different viable source rock intervals are known from previous work and their potential has been confirmed through modelling (this study) for the Adriatic foreland. Results of the numerical simulations indicate that the Triassic shale source rocks reached the oil window by the early Late Cretaceous times, which can be associated with burial during sedimentary deposition (Fig. 10a). The Eocene - Oligocene phase of contraction resulted in the first episode of basin subsidence, and subsequently the Triassic source rocks became overmature. This means that the Triassic shale must have yielded their total hydrocarbon potential by that time. The Cretaceous limestones and shales reached the oil window after the Eocene – Oligocene phase of thrusting of the Dalmatian zone over the Adriatic foreland (Fig. 10b). The maturity of these source rocks started to increase after the deposition of the thick package of Oligocene – Miocene sediments and remained in the oil window until present-day. The Eocene – Oligocene shales also reached the oil window, later, because of basin subsidence and burial associated with the thick sedimentary package of Oligocene to Pliocene age (Fig. 10c). These source rocks reached the gas window in the deepest buried parts below the Dalmatian thrust (Fig. 10e,f).

The main reservoirs in the Adriatic foreland can be assigned to the Cretaceous – Eocene platform carbonates and the Oligocene and Miocene - Pleistocene turbidite intervals (Fig. 4). The presence of hydrocarbons is validated by oil shows that have been found within the JJ-3 well in the Cretaceous-Eocene carbonate sequences at a depth of 4134 m (Bega, 2015; Velaj, 2012) and within the JJ-1 well where gas shows have been encountered in the Oligocene flysch sequence (Velaj, 2012).

Potential seals can be assigned to Neogene shale intervals and low permeable salt layers. The overlying Neogene sediments could have a high sealing capacity, preventing the upward hydrocarbon migration from the Cretaceous and Eocene – Oligocene source rocks. The fluids from the (Triassic?) and Cretaceous source rocks in the Adriatic foreland could migrate through the permeable dolostone and limestone intervals towards the Dalmatian – South Adriatic basin thrust fault (Figs. 5 and 9). These fluids can be blocked by the low permeable layers (e.g., salt) in the hangingwall of this thrust contact. Furthermore, the migration of fluids from these source rocks can be trapped by the overlying low permeability Cenozoic rocks.

5.4.2. Dalmatian zone

Based on the results of the coupled 2D model, the Middle Triassic shales entered the oil window in the Dalmatian zone upon Early Cretaceous times, which can be related to the deposition of the carbonate platform build-ups (Fig. 10d). Soon after the Eocene phase of thrusting of the Budva zone over the Dalmatian zone and the footwall burial, the Triassic source rocks reached the gas window. As a result of this phase of Eocene thrusting and burial of the Dalmatian zone, the Cretaceous limestones and Eocene turbidites entered the oil window, which currently remain in the oil window (Figs. 9e and 10e).

Overlying Cretaceous - Eocene carbonate and Eocene – Oligocene turbidite intervals could serve as potential reservoir rocks (Figs. 4 and 7). Since the Late Miocene onwards, due to the related major structural deformation (see discussion above), these reservoirs could have been charged with oil generated from the Triassic and Cretaceous source rocks. Numerous oil seeps were encountered in Cretaceous carbonates along the Dalmatian coast of Montenegro (Velaj, 2012), indicating a presently active petroleum system.

Potential seal rocks in the Dalmatian zone are found in the overlying Neogene (shale) sediments (Fig. 4). Yet, these sediments were affected by erosion during uplift of the Dalmatian zone (during Late Miocene – Quaternary times), resulting in relatively thin intervals. The hydrocarbons could migrate from their lower structural position towards the higher anticline geometries inside the Dalmatian zone (Fig. 9f), which could represent a structural trap (Spahić et al., 2014). Compared to the South Adriatic basin, the petroleum system potential of the Dalmatian zone is lower due to the thinner overlying Neogene seal rocks, and the absence of overlying impermeable salt layers.

5.4.3. Onshore Dinarides

Within the Budva zone, Triassic and Cretaceous source rocks were simulated to be mature and in the oil window from early Late Cretaceous onwards. The deepest parts of the Triassic source rocks also reached the

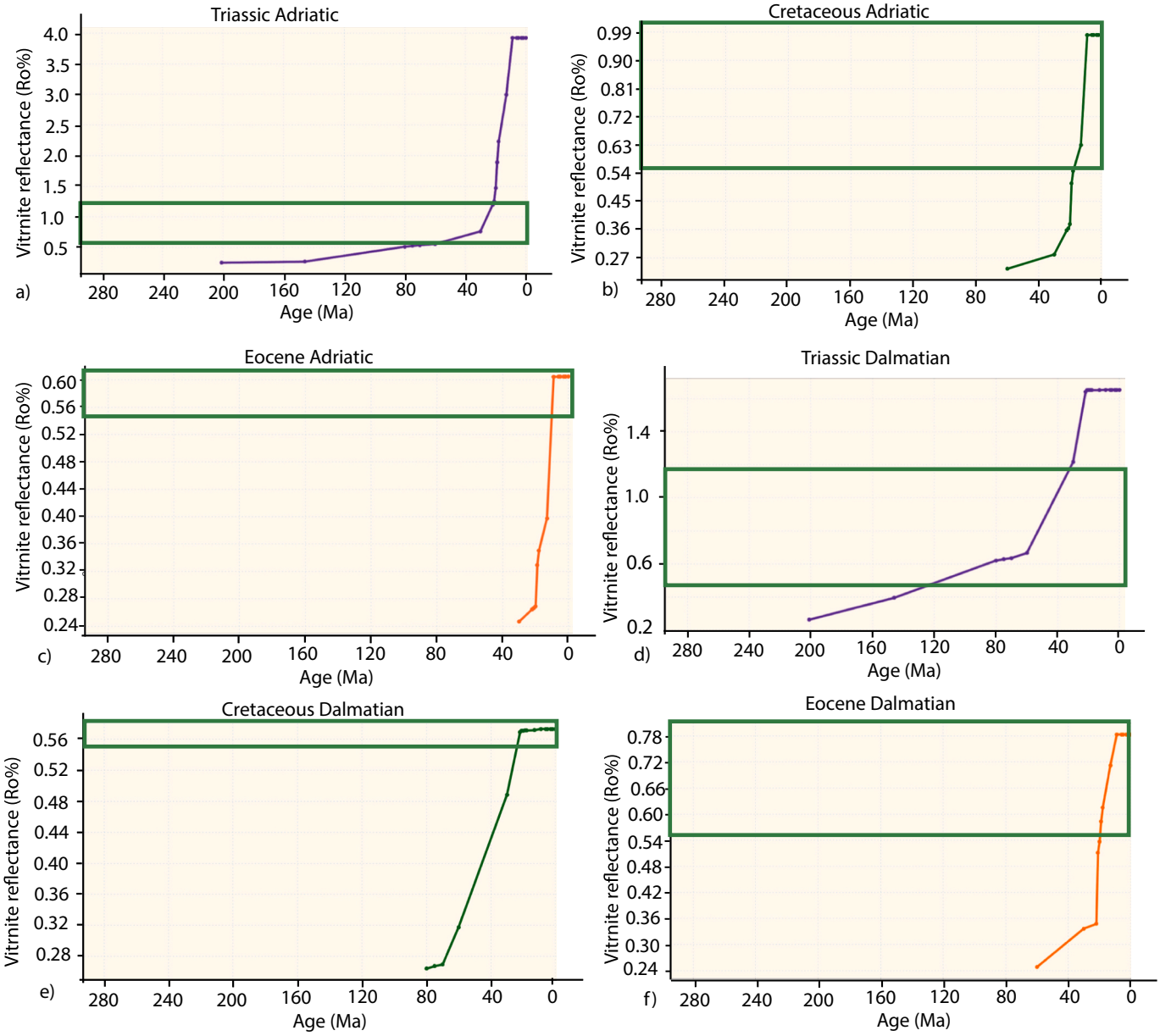

Fig. 10. Timing of simulated maturation of the different source rocks in the: Adriatic basin represented by a) Triassic source rocks that reached the oil window and later became overmature, b) Cretaceous source rocks which reached the oil window, and c) Eocene – Oligocene source rocks that reached the oil window; the Dalmatian zone represented by d) Triassic source rocks that reached the oil and gas window, e) Cretaceous source rocks that reached the oil window, and f) Eocene-Oligocene source rocks that reached the oil window. See location of the source rocks in Fig. 9f. The green rectangles represent the oil window. (For interpretation of the references to colour in this figure legend, the reader is referred to the web version of this article.)

gas window from Late Miocene (Fig. 9e,f). In the area of the High-Karst, Budva and Dalmatian zones, the carbonate rocks must have been affected by meteoric diagenesis (karstification, particularly), when these zones were uplifted after the Eocene – Oligocene (Fig. 9c) and Late Miocene (Fig. 9e) periods of thrusting. Meteoric diagenesis could have enhanced their reservoir properties (porosity and permeability). These carbonate intervals, if sealed, might have been charged by the underlying source rocks after Late Miocene times (when most of the hydrocarbon generation took place). However, as these permeable carbonate rocks locally crop-out at the surface in the Budva and High-Karst units, the sealing capacity within this area is low and the hydrocarbons would have escaped towards the surface (Fig. 9e).

The maturation of the source rocks in the hinterland in the internal parts of the orogen already took place during the build-up of the Triassic – Late Cretaceous platform carbonates. Yet, the latter were exhumed and eroded during the Miocene phase of extension. At present-day the Triassic and Cretaceous source rocks are in the oil and gas windows, and the outcropping (Bosnian-) Durmitor flysch sediments are in the oil window (Fig. 9e). Modelling demonstrates that hydrocarbon generations most probably ended by the Late Cretaceous - Eocene thrusting. The Miocene uplift could have resulted in the escape of the generated hydrocarbons This can be validated by the present-day absence of hydrocarbon seeps at the surface within the Bosnian Flysch zone. Furthermore, the carbonate and turbidite sediments are presently surface-exposed, implying that even if hydrocarbons were trapped in potential reservoirs, such hydrocarbons most likely escaped through the permeable layers towards the surface during recent times.

6. Conclusions

Processes controlling the kinematic and thermal evolution in collisional orogens are inter-related and need to be tackled in a coupled manner in quantitative modelling procedures. This approach was applied through coupled kinematic restoration and thermal basin modelling along one major regional geological section across the Dinarides – example of collisional orogenic belts – and resulted in the following conclusions.

The kinematic restoration of the large-scale structural features resulted in constraining the minimum amounts of shortening, subsidence, sedimentation rates, exhumation, and erosion, which helped, subsequently, in optimizing the structural and geometric configuration of the 2D basin model, allowing pertinent analysis of the thermal distribution and the maturity of potential source rocks during the orogenic evolution. The East-Bosnian Durmitor – Durmitor Flysch contact accommodated ~22 km of shortening during the Late Cretaceous and was associated with *syn*-kinematic deposition of the Durmitor Flysch. During the Eocene – Oligocene phase of contraction, thrusting migrated towards the foreland, accommodating a total amount of ~85 km of shortening mostly by the thrusting of Dalmatian over Adriatic foreland units, resulting in a significant flexural subsidence, syn-kinematic siliciclastic sedimentation, and erosional unconformities. The Late Miocene – Quaternary phase of contraction accommodated a total amount of ~53 km of shortening, which resulted in another major episode of flexural basin subsidence associated with syn-kinematic deposition and the formation of unconformities which is most likely linked to the migrating subduction zone.

High-angle basement involved reverse faults crosscut the structures in the Adriatic foreland and Dalmatian unit, suggesting that a thick-skinned tectonic regime post-dates the thin-skinned emplacement of the Dalmatian unit over the Adriatic foreland. The high-angle basement involved transpressional reverse faults can be interpreted to be a prolongation of an *E*-W oriented transpressive structure of the Middle Adriatic Ridge, which is situated in the middle of the Adriatic Sea.

The constructed kinematic/thermal model together with DoubletCalc tool, helped in proposing preliminary well design and technical performance of a potential geothermal doublet in the Triassic reservoirs of the Durmitor Flysch area, yielding power in the order of 10.07 (P50) and 12.0 MW_{th} (P10). The overlying Cretaceous carbonate reservoirs also yielded encouraging results for developing geothermal energy. These first results indicate a potentially positive business case, particularly for the eastern part of the Dinarides, where hydrocarbon potential has proved to be low. However, it must be noted that detailed studies on the geothermal well design and doublet behaviour need to be refined for the area of interest.

The Eocene – Oligocene and Late Miocene – Quaternary phases of thrusting resulted in the main periods of maturation of Triassic, Cretaceous and Eocene – Oligocene source rocks. Surface heat flow values and the geochemical analysis of limited representative samples of source rocks helped in constraining and confirming the kinematic/thermal model. The South Adriatic basin and Dalmatian zone show the highest petroleum system potential in the study area. In the South Adriatic basin, the Cretaceous limestones and shales reached the oil window after the Eocene – Oligocene thrusting of the Dalmatian zone over the Adriatic foreland and remain in the oil window at present-day. The overlying Eocene – Oligocene shales reached the oil window, and the gas window in the deepest buried parts below the Dalmatian thrust. The Eocene phase of thrusting of the Budva zone over the Dalmatian zone resulted in having the Triassic potential rocks generating gas, while the Cretaceous limestones and Eocene turbidites entered the oil window (until present day).

Declaration of Competing Interest

The authors declare that they have no known competing financial interests or personal relationships that could have appeared to influence the work reported in this paper.

Data availability

No data was used for the research described in the article.

Acknowledgements

This study was financed by IFP Energies Nouvelles, France and University of Utrecht, The Netherlands. The Montenegro Seismological Observatory and Montenegro Hydrocarbon Administration are gratefully acknowledged for providing access to subsurface information in the offshore Montenegro. The excellent suggestions and comments made by two reviewers and the Editor have significantly improved the original manuscript and are very much acknowledged.

References

Andrić, N., Sant, K., Matenco, L., Mandic, O., Tomljenović, B., Pavelić, D., Hrvatović, H., Demir, V., Ooms, J., 2017. The link between tectonics and sedimentation in asymmetric extensional basins: inferences from the study of the Sarajevo-Zenica Basin. Mar. Pet. Geol. 83, 305–332. https://doi.org/10.1016/j.marpetgeo.2017.02.024.

Ballato, P., Brune, S., Strecker, M.R., 2019. Sedimentary loading–unloading cycles and faulting in intermontane basins: Insights from numerical modeling and field observations in the NW Argentine Andes. Earth Planet. Sci. Lett. 506, 388–396. https://doi.org/10.1016/j.epsl.2018.10.043.

Balling, P., Grützner, C., Tomljenović, B., Spakman, W., Ustaszewski, K., 2021a. Post-collisional mantle delamination in the Dinarides implied from staircases of Oligo-Miocene uplifted marine terraces. Sci. Rep. 11 (1), 2685. https://doi.org/10.1038/s41598-021-81561-5.

Balling, P., Tomljenović, B., Schmid, S.M., Ustaszewski, K., 2021b. Contrasting along-strike deformation styles in the central external Dinarides assessed by balanced cross-sections: implications for the tectonic evolution of its Paleogene flexural foreland basin system. Glob. Planet. Chang. 103587 https://doi.org/10.1016/j.gloplacha.2021.103587.

Bally, A.W., 1981. Thoughts on the tectonics of folded belts. Geol. Soc. Spec. Publ. 9, 13–32. https://doi.org/10.1144/GSL.SP.1981.009.01.03.

Barker, C.E., Pawlewicz, M.J., 1986. The correlation of vitrinite reflectance with maximum temperature in humic organic matter. In: Buntebarth, G., Stegena, L. (Eds.), Paleogeothermics, Lecture Notes in Earth Sciences, vol. 5. Springer, Berlin, Heidelberg, pp. 77–93.

Beaumont, C., 1981. Foreland basins. Geophys. J. Int. 65 (2), 291–329. https://doi.org/10.1111/j.1365-246X.1981.tb02715.x.

Beaumont, C., Fullsack, P., Willet, S., Hamilton, J., Johnson, D., Ellis, S., Platon, M., 1990. Coupling climate, surface processes and tectonics in orogens and their associated sedimentary basins. In: Hall, J. (Ed.), Lithoprobe East: Report of Transect Meeting, 1990. Memorial University, St. John's.

Bega, Z., 2015. Hydrocarbon exploration potential of Montenegro - a brief review. J. Pet. Geol. 38 (3), 317–330. https://doi.org/10.1111/jpg.12613.

Bennett, R.A., Hreinsdóttir, S., Buble, G., Bašić, T., Bačić, Ž., Marjanović, M., Casale, G., Gendaszek, A., Cowan, D., 2008. Eocene to present subduction of Southern Adria mantle lithosphere beneath the Dinarides. Geology 36 (1), 3–6. https://doi.org/10.1130/G24136A.1.

Bertotti, G., Picotti, V., Chilovi, C., Fantoni, R., Merlini, S., Mosconi, A., 2001. Neogene to Quaternary sedimentary basins in the south Adriatic (Central Mediterranean): foredeeps and lithospheric buckling. Tectonics 20 (5), 771–787. https://doi.org/10.1029/2001TC900012.

Boersma, Q.D., Bruna, P.O., de Hoop, S., Vinci, F., Moradi Tehrani, A., Bertotti, G., 2021. The impact of natural fractures on heat extraction from tight Triassic sandstones in the West Netherlands Basin: a case study combining well, seismic and numerical data. Geol. Mijnb./Neth. J. Geosci. 100, e6 https://doi.org/10.1017/njg.2020.21.

Bonacci, O., 2017. Preliminary analysis of the decrease in water level of Vrana Lake on the small carbonate island of Cres (Dinaric karst, Croatia). Geol. Soc. Spec. Publ. 466, 307–317. https://doi.org/10.1144/SP466.6.

Borojević Šoštarić, S., Kulušić, A., 2014. Dinaride evaporite mélange: Diagenesis of the Kosovo Polje evaporites. Geol. Croat. 67 (1), 59–74. https://doi.org/10.4154/GC.2014.05.

Cadjenovic, D., Kilibarda, Z., Radulovic, N., 2008. Late Triassic to Late Jurassic evolution of the Adriatic Carbonate Platform and Budva Basin, Southern Montenegro. Sediment. Geol. 204 (1–2), 1–17. https://doi.org/10.1016/j.sedgeo.2007.12.005.

Clauzon, G., 1990. Restitution de l'évolution géodynamique néogène du bassin du Roussillon et de l'unité adjacente des Corbières d'après les données écostratigraphiques et paléogéographiques. Paléobiol. Cont. 17, 125–155.

Cornu, T., Schneider, F., Gratier, J.P., 2003. 3D discrete kinematic modelling applied to extensional and compressional tectonics. Geol. Soc. Spec. Publ. 212 (1), 285–294. https://doi.org/10.1144/GSL.SP.2003.212.01.19.

Crne, A.E., Weissert, H., Gorican, S., Bernasconi, S.M., 2011. A biocalcification crisis at the Triassic-Jurassic boundary recorded in the Budva Basin (Dinarides, Montenegro). Geol. Soc. Am. Bull. 123 (1–2), 40–50. https://doi.org/10.1130/B30157.1.

D'Agostino, N., Métois, M., Koci, R., Duni, L., Kuka, N., Ganas, A., Georgiev, I., Jouanne, F., Kaludjerovic, N., Kandić, R., 2020. Active crustal deformation and rotations in the southwestern Balkans from continuous GPS measurements. Earth Planet. Sci. Lett. 539, 116246 https://doi.org/10.1016/j.epsl.2020.116246.

Dahlstrom, C.D.A., 1969. Balanced cross-sections. Can. J. Earth Sci. 6 (4), 743–757. https://doi.org/10.1139/e69-069.

Davy, P., Gillet, P., 1986. The stacking of thrust slices in collision zones and its thermal consequences. Tectonics 5 (6), 913–929. https://doi.org/10.1029/TC005i006p00913.

de Leeuw, A., Mandic, O., Krijgsman, W., Kuiper, K., Hrvatović, H., 2012. Paleomagnetic and geochronologic constraints on the geodynamic evolution of the Central Dinarides. Tectonophysics 530-531, 286–298. https://doi.org/10.1016/j.tecto.2012.01.004.

Demetrescu, C., Andreescu, M., 1994. On the thermal regime of some tectonic units in a continental collision environment in Romania. Tectonophysics 230 (3–4), 265–276. https://doi.org/10.1016/0040-1951(94)90140-6.

Dezes, P., Schmid, S.M., Ziegler, P.A., 2004. Evolution of the European Cenozoic Rift System: interaction of the Alpine and Pyrenean orogens with their foreland lithosphere. Tectonophysics 389 (1–2), 1–33. https://doi.org/10.1016/j.tecto.2004.06.011.

Dimitrijević, M.D., 1997. Geology of Yugoslavia, 2nd edition. Geoinstitute, Belgrade, Belgrade, p. 187.

Do Couto, D., Garel, S., Moscariello, A., Bou Daher, S., Littke, R., Weniger, P., 2021. Origins of hydrocarbons in the Geneva Basin: insights from oil, gas and source rock organic geochemistry. Swiss J. Geosci. 114 (1), 11. https://doi.org/10.1186/s00015-021-00388-4.

Doglioni, C., Carminati, E., Cuffaro, M., Scrocca, D., 2007. Subduction kinematics and dynamic constraints. Earth-Sci. Rev. 83 (3–4), 125–175. https://doi.org/10.1016/j.earscirev.2007.04.001.

Dragasević, T., 1983. Oil geological exploration in the Montenegro Offshore in Yugoslavia. Nafta 34 (7–8), 397–404.

Dubljević, V., 2008. Oil and gas in Montenegro, Ministry for Economic Development, Government of Montenegro. In: Geological Survey of Montenegro, 19. https://wapi.gov.me/download/70259591-4f7e-43fb-9058-12d7a4f4fea5?version=1.0.

Duretz, T., Gerya, T.V., 2013. Slab detachment during continental collision: influence of crustal rheology and interaction with lithospheric delamination. Tectonophysics 602, 124–140. https://doi.org/10.1016/j.tecto.2012.12.024.

Ellouz, N., Roure, F., Săndulescu, M., Bădescu, D., 1994. Balanced cross sections in the Eastern Carpathians (Romania): A tool to quantify Neogene dynamics. In: Roure, F., Ellouz, N., Shein, V.S., Skvortsov, I. (Eds.), Geodynamic Evolution of Sedimentary Basins, International Symposium Moskow 1992 Proceedings. Technip, Paris, pp. 305–325.

England, P., Houseman, G., 1986. Finite strain calculations of continental deformation, 2, comparison with the India-Eurasian collision. J. Geophys. Res. 91, 3664–3676. https://doi.org/10.1029/JB091iB03p03664.

Espitalié, J., Laporte, J.L., Madec, M., Marquis, F., Leplat, P., Paulet, J., Boutefeu, A., 1977. Méthode rapide de caractérisation des roches mères, de leur potentiel pétrolier et de leur degré d'évolution. Rev. Inst. fr. pét. 32, 23–42.

Faccenna, C., Becker, T.W., 2020. Topographic expressions of mantle dynamics in the Mediterranean. Earth-Sci. Rev. 209, 103327 https://doi.org/10.1016/j.earscirev.2020.103327.

Ferket, H., Guilhaumou, N., Roure, F., Swennen, R., 2011. Insights from fluid inclusions, thermal and PVT modeling for paleo-burial and thermal reconstruction of the Córdoba petroleum system (NE Mexico). Mar. Pet. Geol. 28 (4), 936–958. https://doi.org/10.1016/j.marpetgeo.2010.01.020.

Goričan, S., 1994. Jurassic and Cretaceous Radiolarian Biostratigraphy and Sediemntary Evolution of the Budva Zone (Dinarides, Montenegro). Memoires de Geologie, 18. Université de Lausanne, Lausanne, 177 pp.

Goričan, Š., Košir, A., Rožič, B., Šmuc, A., Gale, L., Kukoč, D., Celarc, B., Črne, A.E., Kolar-Jurkovšek, T., Placer, L., 2012. Mesozoic deep-water basins of the eastern Southern Alps (NW Slovenia). J. Alp. Geol. 55, 1–44.

Gorini, C., Lofi, J., Duvail, C., dos Reis, A.T., Guennoc, P., Le Strat, P., Mauffret, A., 2005. The Late Messinian salinity crisis and Late Miocene tectonism: interaction and consequences on the physiography and post-rift evolution of the Gulf of Lions margin. Mar. Pet. Geol. 22 (6–7), 695–712. https://doi.org/10.1016/j.marpetgeo.2005.03.012.

Grandić, S., Kratkovic, I., Rusan, I., 2010. Hydrocarbon potential assesment of the slope deposits along the SW Dinarides carbonate platform edge. Nafta 61, 325–338.

Grenerczy, G., Sella, G., Stein, S., Kenyeres, A., 2005. Tectonic implications of the GPS velocity field in the Northern Adriatic region. Geophys. Res. Lett. 32, 1–4. https://doi.org/10.1029/2005GL022947.

Gušić, I., Jelaska, V., 1993. Upper Cenomanian – Lower Turonian sea-level rise and its consequences on the Adriatic-Dinaric carbonate platform. Geol. Rundsch. 82, 676–686. https://doi.org/10.1007/BF00191495.

Handy, M.R., Giese, J., Schmid, S.M., Pleuger, J., Spakman, W., Onuzi, K., Ustaszewski, K., 2019. Coupled crust-mantle response to slab tearing, bending, and rollback along the Dinaride-Hellenide Orogen. Tectonics 38 (8), 2803–2828. https://doi.org/10.1029/2019TC005524.

Haq, B., Gorini, C., Baur, J., Moneron, J., Rubino, J.-L., 2020. Deep Mediterranean's Messinian evaporite giant: how much salt? Glob. Planet. Chang. 184, 103052 https://doi.org/10.1016/j.gloplacha.2019.103052.

Harzhauser, M., Mandic, O., 2008. Neogene lake systems of Central and South-Eastern Europe: Faunal diversity, gradients and interrelations. Palaeogeogr. Palaeoclimatol. Palaeoecol. 260 (3–4), 417–434. https://doi.org/10.1016/j.palaeo.2007.12.013.

Harzhauser, M., Mandic, O., Latal, C., Kern, A., 2012. Stable isotope composition of the Miocene Dinaride Lake System deduced from its endemic mollusc fauna. Hydrobiologia 682 (1), 27–46. https://doi.org/10.1007/s10750-011-0618-3.

Hrvatović, H., 2006. Geological Guidebook through Bosnia and Herzegovina. Geological Survey of Federation Bosnia and Herzegovina, Sarajevo, 162 pp.

Hrvatović, H., Pamić, J., 2005. Principal thrust-nappe structures of the Dinarides. Acta Geol. Hung. 48 (2), 133–151. https://doi.org/10.1556/ageol.48.2005.2.4.

Huerta, A.D., Rodgers, D.W., 2006. Constraining rates of thrusting and erosion: insights from kinematic thermal modeling. Geology 34 (7), 541–544. https://doi.org/10.1130/G22421.1.

Jolivet, L., Menant, A., Roche, V., Le Pourhiet, L., Maillard, A., Augier, R., Do Couto, D., Gorini, C., Thinon, I., Canva, A., 2021. Transfer zones in Mediterranean back-arc regions and tear faults. BSGF - Earth Sci. Bull. 192 (11) https://doi.org/10.1051/bsgf/2021006.

Korbar, T., 2009. Orogenic evolution of the External Dinarides in the NE Adriatic region: a model constrained by tectonostratigraphy of Upper Cretaceous to Paleogene carbonates. Earth-Sci. Rev. 96 (4), 296–312. https://doi.org/10.1016/j.earscirev.2009.07.004.

Lachenbrach, A., 1970. Crustal temperature and heat productivity implications on the linear heat flow relation. J. Geophys. Res. 75 (17), 3291–3300. https://doi.org/10.1029/JB075i017p03291.

Lancaster, P., Salkauskas, K., 1981. Surfaces generated by moving least-squares methods. Math. Comput. 37 (155), 141–158. https://doi.org/10.2307/2007507.

Leloup, P.H., Ricard, Y., Battaglia, J., Lacassin, R., 1999. Shear heating in continental strike-slip shear zones:model and field examples. Geophys. J. Int. 136 (1), 19–40. https://doi.org/10.1046/j.1365-246X.1999.00683.x.

Limberger, J., Calcagno, P., Manzella, A., Trumpy, E., Boxem, T., Pluymaekers, M.P.D., van Wees, J.D., 2014. Assessing the prospective resource base for enhanced geothermal systems in Europe. Geoth. Energ. Sci. 2, 55–71. https://doi.org/10.5194/gtes-2-55-2014.

Mandic, O., de Leeuw, A., Bulić, J., Kuiper, K.F., Krijgsman, W., Jurišić-Polšak, Z., 2012. Paleogeographic evolution of the Southern Pannonian Basin: 40Ar/39Ar age constraints on the Miocene continental series of Northern Croatia. Int. J. Earth Sci. 101, 1033–1046. https://doi.org/10.1007/s00531-011-0695-6.

Matenco, L., Radivojević, D., 2012. On the formation and evolution of the Pannonian Basin: Constraints derived from the structure of the junction area between the Carpathians and Dinarides. Tectonics 31 (6). https://doi.org/10.1029/2012TC003206.

Mazzuca, N., Bruni, A., Joppen, T., 2015. Exploring the potential of deep targets in the South Adriatic Sea: insight from 2D basin modelling of the Croatian offshore. Geol. Croat. 68 (3), 237–246. https://doi.org/10.4154/GC.2015.18.

Métois, M., D'Agostino, N., Avallone, A., Chamot-Rooke, N., Rabaute, A., Duni, L., Kuka, N., Koci, R., Georgiev, I., 2015. Insights on continental collisional processes from GPS data: dynamics of the peri-Adriatic belts. J. Geophys. Res. Solid Earth 120 (12), 8701–8719. https://doi.org/10.1002/2015JB012023.

Mikes, T., Christ, D., Petri, R., Dunkl, I., Frei, D., Báldi-Beke, M., Reitner, J., Wemmer, K., Hrvatović, H., von Eynatten, H., 2008. Provenance of the Bosnian Flysch. Swiss J. Geosci. 101 (1), 31–54. https://doi.org/10.1007/s00015-008-1291-z.

Milivojević, M.G., 1993. Geothermal model of the earths crust and lithosphere for the territory of Yugoslavia: some tectonic implications. Stud. Geophys. Geod. 37, 265–278. https://doi.org/10.1007/BF01624600.

Milivojević, M., Martinović, M., 2005. Geothermal Energy Possibilities, Exploration and Future Prospects in Serbia. World Geothermal Congress, Antalya, Turkey, p. 11.

Miošić, N., Samardžić, N., Hrvatović, H., 2010. The Current Status of Geothermal Energy Use and Development in Bosnia and Herzegovina. World Geothermal Congress, Bali, Indonesia, p. 11.

Mitra, G., Boyer, S.E., 1986. Energy-balance and deformation mechanisms of duplexes. J. Struct. Geol. 8 (3–4), 291–304. https://doi.org/10.1016/0191-8141(86)90050-7.

Moulin, A., Benedetti, L., Rizza, M., Jamšek Rupnik, P., Gosar, A., Bourlès, D., Keddadouche, K., Aumaître, G., Arnold, M., Guillou, V., Ritz, J.-F., 2016. The Dinaric fault system: large-scale structure, rates of slip, and Plio-Pleistocene evolution of the transpressive northeastern boundary of the Adria microplate. Tectonics 35 (10), 2258–2292. https://doi.org/10.1002/2016TC004188.

Mrinjek, E., 1993. Sedimentology and depositional setting of alluvial Promina Beds in Northern Dalmatia. Geol. Croat. 46 (2), 243–261.

Nemčok, M., Schamel, S., Gayer, R.A., 2005. Thrustbelts: Structural Architecture, Thermal Regimes and Petroleum Systems. Cambridge University Press, Cambridge, p. 541.

Picha, F., 2002. Late orogenic strike-slip faulting and escape tectonics in frontal Dinarides-Hellenides, Croatia, Yugoslavia, Albania, and Greece. AAPG Bull. 86 (9), 1659–1671. https://doi.org/10.1306/61EEDD32-173E-11D7-8645000102C1865D.

Platt, J.P., 1986. Dynamics of orogenic wedges and the uplift of high-pressure metamorphic rocks. AAPG Bull. 97 (9), 1037–1053.

Porkoláb, K., Kövér, S., Benkó, Z., Héja, G.H., Fialowski, M., Soós, B., Spajić, N.G., Đerić, N., Fodor, L., 2019. Structural and geochronological constraints from the Drina-Ivanjica thrust sheet (Western Serbia): implications for the Cretaceous–Paleogene tectonics of the Internal Dinarides. Swiss J. Geosci. 112, 217–234. https://doi.org/10.1007/s00015-018-0327-2.

Ravnik, D., Rajver, D., Poljak, M., Živčić, M., 1995. Overview of the geothermal field of Slovenia in the area between the Alps, the Dinarides and the Pannonian basin. Tectonophysics 250 (1–3), 135–149. https://doi.org/10.1016/0040-1951(95)00031-X.

Robertson, A., Karamata, S., Saric, K., 2009. Overview of ophiolites and related units in the Late Palaeozoic-Early Cenozoic magmatic and tectonic development of Tethys in the northern part of the Balkan region. Lithos 108 (1–4), 1–36. https://doi.org/10.1016/j.lithos.2008.09.007.

Rosenberg, C.L., Schneider, S., Scharf, A., Bertrand, A., Hammerschmidt, K., Rabaute, A., Brun, J.P., 2018. Relating collisional kinematics to exhumation processes in the Eastern Alps. Earth-Sci. Rev. 176, 311–344. https://doi.org/10.1016/j.earscirev.2017.10.013.

Roure, F., Bessereau, G., Kotarba, M., Kuśmierek, J., Strzetelski, W., 1993. Structure and hydrocarbon habitats of the Polish Carpathian Province. AAPG Bull. 77 (9), 1660. https://doi.org/10.1306/BDFF84E8-1718-11D7-8645000102C1865D.

Roure, F., Fili, I., Najaz, S., Cadet, J.P., Mushka, K., Bonneau, M., 2004. Kinematic evolution and petroleum systems—An appraisal of the outer albanides. In: McClay, K.R. (Ed.), Thrust Tectonics and Hydrocarbon Systems, AAPG Memoir, vol. 82, pp. 474–493.

Roure, F., Swennen, R., Schneider, F., Faure, J.-L., Ferket, H., Guilhaumou, N., Osadetz, K., Robion, P., Vandeginste, V., 2005. Incidence and importance of tectonics and natural fluid migration on reservoir evolution in foreland fold-and-thrust belts. Oil Gas Sci. Technol. 60, 67–106. https://doi.org/10.2516/ogst:2005006.

Royden, L.H., 1993. The tectonic expression of slab pull at continental convergent boundaries. Tectonics 12 (2), 303–325. https://doi.org/10.1029/92TC02248.

Schmid, S., Bernoulli, D., Fügenschuh, B., Matenco, L., Schefer, S., Schuster, R., Tischler, M., Ustaszewski, K., 2008. The Alpine-Carpathian-Dinaridic orogenic system: correlation and evolution of tectonic units. Swiss J. Geosci. 101, 139–183. https://doi.org/10.1007/s00015-008-1247-3.

Schmid, S.M., Fügenschuh, B., Kounov, A., Maţenco, L., Nievergelt, P., Oberhänsli, R., Pleuger, J., Schefer, S., Schuster, R., Tomljenović, B., Ustaszewski, K., van Hinsbergen, D.J.J., 2020. Tectonic units of the Alpine collision zone between Eastern Alps and western Turkey. Gondwana Res. 78, 308–374. https://doi.org/10.1016/j.gr.2019.07.005.

Schmitz, B., Biermanns, P., Hinsch, R., Đaković, M., Onuzi, K., Reicherter, K., Ustaszewski, K., 2020. Ongoing shortening in the Dinarides fold-and-thrust belt: a new structural model of the 1979 (Mw 7.1) Montenegro earthquake epicentral region. J. Struct. Geol. 141, 104192 https://doi.org/10.1016/j.jsg.2020.104192.

Schneider, F., 2003. Basin modeling in Complex Area: examples from Eastern Venezuelan and Canadian Foothills. Oil Gas Sci. Technol. 58 (2), 313–324. https://doi.org/10.2516/ogst:2003019.

Scisciani, V., Calamita, F., 2009. Active intraplate deformation within Adria: examples from the Adriatic Region. Tectonophysics 476 (1–2), 57–72. https://doi.org/10.1016/j.tecto.2008.10.030.

Spahić, D., Wygrala, B., Rundić, L., 2014. A few remarks on hydrocarbon resource assessment within the Dinaric thrust and fold belt. Nafta 3, 244–249.

Spooner, C., Scheck-Wenderoth, M., Cacace, M., Götze, H.-J., Luijendijk, E., 2020. The 3D thermal field across the Alpine orogen and its forelands and the relation to seismicity. Glob. Planet. Chang. 193, 103288 https://doi.org/10.1016/j.gloplacha.2020.103288.

Stampfli, G.M., Borel, G.D., 2002. A plate tectonic model for the Paleozoic and Mesozoic constrained by dynamic plate boundaries and restored synthetic oceanic isochrons. Earth Planet. Sci. Lett. 196 (1–2), 17–33. https://doi.org/10.1016/S0012-821X(01)00588-X.

Stojadinovic, U., Matenco, L., Andriessen, P., Toljić, M., Rundić, L., Ducea, M.N., 2017. Structure and provenance of Late Cretaceous–Miocene sediments located near the NE Dinarides margin: inferences from kinematics of orogenic building and subsequent extensional collapse. Tectonophysics 710–711, 184–204. https://doi.org/10.1016/j.tecto.2016.12.021.

Šumanovac, F., 2010. Lithosphere structure at the contact of the Adriatic microplate and the Pannonian segment based on the gravity modelling. Tectonophysics 485 (1–4), 94–106. https://doi.org/10.1016/j.tecto.2009.12.005.

Sweeney, J.J., Burnham, A.K., 1990. Evaluation of a simple model of vitrinite reflectance based on chemical kinetics. AAPG Bull. 74 (10), 1559–1570. https://doi.org/10.1306/0C9B251F-1710-11D7-8645000102C1865D.

Tapponnier, P., Peltzer, G., Armijo, R., 1986. On the mechanics of the collision between India and Asia. Geol. Soc. Spec. Publ. 19, 115–157. https://doi.org/10.1144/GSL.SP.1986.019.01.07.

Tari, V., 2002. Evolution of the northern and western Dinarides: a tectonostratigraphic approach. Stephan Mueller Spec. Publ. Ser. 1, 223–236. https://doi.org/10.5194/smsps-1-223-2002.

Teichmüller, M., Durand, B., 1983. Fluorescence microscopical rank studies on liptinites and vitrinites in peat and coals, and comparison with results of the rock-eval pyrolysis. Int. J. Coal Geol. 2 (3), 197–230. https://doi.org/10.1016/0166-5162(83)90001-0.

Tišljar, J., 1992. Origin and depositional environments of the evaporite and carbonate complex (Upper Permian) from the Central Part of the Dinarides (Southern Croatia and Western Bosnia). Geol. Croat. 45 (1), 115–126. https://doi.org/10.4154/GC.1992.09.

Tomljenović, B., Csontos, L., Márton, E., Márton, P., 2008. Tectonic evolution of the northwestern Internal Dinarides as constrained by structures and rotation of Medvednica Mountains, North Croatia. Geol. Soc. Spec. Publ. 298 (1), 145–167. https://doi.org/10.1144/SP298.8.

Turrini, C., Bosica, B., Ryan, P., Shiner, P., Lacombe, O., Roure, F., 2017. 3D structural and thermal modelling of Mesozoic petroleum systems in the Po Valley Basin, northern Italy. Pet. Geosci. 24 (2), 172–196. https://doi.org/10.1144/petgeo2017-031.

Ungerer, P., 1990. State of the art of research in kinetic modelling of oil formation and expulsion. Org. Geochem. 16 (1–3), 1–25. https://doi.org/10.1016/0146-6380(90)90022-R.

Ustaszewski, K., Kounov, A., Schmid, S.M., Schaltegger, U., Krenn, E., Frank, W., Fügenschuh, B., 2010. Evolution of the Adria-Europe plate boundary in the northern Dinarides: from continent-continent collision to back-arc extension. Tectonics 29 (6), TC6017. https://doi.org/10.1029/2010TC002668.

van Krevelen, D.W., 1950. Graphical-statistical method for the study of structure and reaction processes of coal. Fuel 29, 269–284.

van Unen, M., Matenco, L., Demir, V., Nader, F.H., Darnault, R., Mandic, O., 2019a. Transfer of deformation during indentation: inferences from the post- middle Miocene evolution of the Dinarides. Glob. Planet. Chang. 182, 103027 https://doi.org/10.1016/j.gloplacha.2019.103027.

van Unen, M., Matenco, L., Nader, F.H., Darnault, R., Mandic, O., Demir, V., 2019b. Kinematics of foreland-vergent crustal accretion: inferences from the Dinarides evolution. Tectonics 38 (1), 49–76. https://doi.org/10.1029/2018TC005066.

van Wees, J.D., Kronimus, A., van Putten, M., Pluymaekers, P.P.D., Mijnlieff, H., van Hooff, P., Obdam, A., Kramers, L., 2012. Geothermal aquifer performance assessment for direct heat production - methdodology and application to Rotliegend aquifers. Neth. J. Geosci. 91 (4), 651–665. https://doi.org/10.1017/S0016774600000433.

Velaj, T., 2012. Tectonic style and hydrocarbon evaluation of duplex Kruja zone in Albania. Nafta 63 (7–8), 236–242.

Velaj, T., 2015. The structural style and hydrocarbon exploration of the subthrust in the Berati Anticlinal Belt, Albania. J. Petrol. Explor. Prod. Technol. 5, 123–145. https://doi.org/10.1007/s13202-015-0162-1.

Velić, J., Malvić, T., Cvetković, M., Velić, I., 2015. Stratigraphy and petroleum geology of the Croatian part of the Adriatic Basin. J. Pet. Geol. 38 (3), 281–300. https://doi.org/10.1111/jpg.12611.

Verges, J., Millan, H., Roca, E., Munoz, J.A., Marzo, M., Cires, J., Den, B.T., Zoetemeijer, R., Cloetingh, S., 1995. Eastern Pyrenees and related foreland basins; pre-, syn- and post-collisional crustal-scale cross-sections. Mar. Pet. Geol. 12 (8), 903–915. https://doi.org/10.1016/0264-8172(95)98854-X.

Vilasi, N., Malandain, J., Barrier, L., Callot, J.-P., Amrouch, K., Guilhaumou, N., Lacombe, O., Muska, K., Roure, F., Swennen, R., 2009. From outcrop and petrographic studies to basin-scale fluid flow modelling: the use of the Albanian natural laboratory for carbonate reservoir characterisation. Tectonophysics 474 (1–2), 367–392. https://doi.org/10.1016/j.tecto.2009.01.033.

Vlahovic, I., Tisljar, J., Velic, I., Maticec, D., 2005. Evolution of the Adriatic Carbonate Platform: palaeogeography, main events and depositional dynamics. Palaeogeogr. Palaeoclimatol. Palaeoecol. 220 (3–4), 333–360. https://doi.org/10.1016/j.palaeo.2005.01.011.

Vogt, K., Matenco, L., Cloetingh, S., 2017. Crustal mechanics control the geometry of mountain belts. Insights from numerical modelling. Earth Planet. Sci. Lett. 460, 12–21. https://doi.org/10.1016/j.epsl.2016.11.016.

Vrabec, M., Fodor, L., 2005. Late Cenozoic tectonics of Slovenia: structural styles at the Northeastern corner of the Adriatic microplate. In: Pinter, N., Grenerczy, G., Weber, J., Stein, S., Medak, D. (Eds.), The Adria Microplate: GPS Geodesy, Tectonics and Hazards. Nato Science Series: IV: Earth and Environmental Sciences. Springer Verlag, pp. 151–168.

Weber, J., Vrabec, M., Pavlovcic-Preseren, P., Dixon, T., Jiang, Y., Stopar, B., 2010. GPS-derived motion of the Adriatic microplate from Istria Peninsula and Po Plain sites, and geodynamic implications. Tectonophysics 483 (3–4), 214–222. https://doi.org/10.1016/j.tecto.2009.09.001.

Willett, S.D., Brandon, M.T., 2002. On steady states in mountain belts. Geology 30 (2), 175–178. https://doi.org/10.1130/0091-7613(2002)030<0175:OSSIMB>2.0.CO;2.

Wortel, M.J.R., Spakman, W., 1992. Structure and dynamics of subducted lithosphere in the Mediterranean region. Proc. K. Ned. Akad. Wet. 95, 325–347. https://dspace.library.uu.nl/handle/1874/349369.

Wortel, M.J.R., Spakman, W., 2000. Subduction and slab detachment in the Mediteranean-Carpathian Region. Science 290, 1910–1917. https://doi.org/10.1126/science.290.5498.1910.

Zappaterra, E., 1994. Source-rock distribution of the periadriatic region. AAPG Bull. 78 (3), 333–354. https://doi.org/10.1306/BDFF90A0-1718-11D7-8645000102C1865D.

Žibret, L., Vrabec, M., 2016. Palaeostress and kinematic evolution of the orogen-parallel NW-SE striking faults in the NW external Dinarides of Slovenia unraveled by mesoscale fault-slip data analysis. Geol. Croat. 69 (3), 295–305. https://doi.org/10.4154/gc.2016.30.

Zoetemeijer, R., Cloetingh, S., Sassi, W., Roure, F., 1993. Modelling of piggyback modelling of piggyback-basin stratigraphy: record of tectonic evolution. Tectonophysics 226 (1–4), 253–269. https://doi.org/10.1016/0040-1951(93)90121-Y.

Zupanič, J., Babić, L., 2011. Sedimentary evolution of an inner foreland basin margin: Paleogene Promina Beds of the type area, Mt. Promina (Dinarides, Croatia). Geol. Croat. 64 (2), 101–120. https://doi.org/10.4154/GC.2011.09.